Charge-transfer materials for electrochemical water desalination, ion separation and the recovery of elements

Pattarachai Srimuk[1,2], *Xiao Su*[3], *Jeyong Yoon*[4,5,6], *Doron Aurbach*[7] *and Volker Presser*[1,2]✉

Abstract | Reversible electrochemical processes are a promising technology for energy-efficient water treatment. Electrochemical desalination is based on the compensation of electric charge by ionic species, through which the ions are immobilized and, thereby, removed from a feed-water stream flowing through a desalination cell. For decades, electrochemical desalination has focused on the use of carbon electrodes, but their salt-removal ability is limited by the mechanism of ion electrosorption at low molar concentrations and low charge-storage capacity. Recently, charge-transfer materials, often found in batteries, have demonstrated much larger charge-storage capacities and energy-efficient desalination at both low and high molar strengths. In this Review, we assess electrochemical-desalination mechanisms and materials, including ion electrosorption and charge-transfer processes, namely, ion binding with redox-active polymers, ion insertion, conversion reactions and redox-active electrolytes. Furthermore, we discuss performance metrics and cell architectures, which we decouple from the nature of the electrode material and the underlying mechanism to show the versatility of cell-design concepts. These charge-transfer processes enable a wealth of environmental applications, ranging from potable-water generation and industrial-water remediation to lithium recovery and heavy-metal-ion removal.

The energy-efficient removal of ions from saline media is central to a sustainable future with clean water and renewable energy[1]. Although the focus is on the generation of potable water, desalination and ion separation are equally important to the manufacturing, agricultural and mining industries[2]. Present-day, large-scale water purification and treatment mostly employ thermal desalination or reverse osmosis (membrane-based desalination)[3]. Although reliable and effective, the growing demand for water remediation necessitates cheaper and more sustainable technologies with a lower energy footprint. Electrochemical processes, known for their cyclic efficiency and reversibility, are attractive for next-generation water treatment and purification. Capacitive-deionization (CDI) technologies use electric charge to remove ions. As the electric charge — and energy — is not lost but (partially) recovered during the cyclic operation, such devices have dual use as desalination and energy-storage units[4].

Reversible electrochemical desalination, later termed CDI, was introduced by Blair and Murphy in 1960 (REF.[5]). This early work used a carbon-based material as the sodium-ion-removal electrode and an Ag/AgCl electrode for chloride removal[5]. In 1967, Murphy and Caudle replaced Ag/AgCl with a carbon electrode to create the first carbon–carbon CDI cell[6]. In 1971, Johnson and Newman identified that the double-layer capacity limits the ion-electrosorption capacity of carbon electrodes, owing to its strong influence on the available surface area and the applied potential[7]. Soon after, the Gouy–Chapman–Stern theory was implemented to quantify the influence of pore size, carbon surface area and feed concentration on desalination performance[8–11]. For microporous carbon, especially with pore sizes <1 nm, the Gouy–Chapman–Stern model no longer adequately describes the experimental results, owing to the overlap of the electrical double layers. The modified Donnan model[12] more accurately describes electrical double-layer formation in such micropores and can be used as a basis to model CDI desalination[13–15]. However, the use of nanoporous carbon electrodes remains limited by the moderate charge-storage capacity of carbon

✉e-mail: volker.presser@leibniz-inm.de

https://doi.org/10.1038/s41578-020-0193-1

materials (~100–200 F g^{-1})[16] and the failure to afford permselective ion removal at high molar strength[17]. Even in the uncharged state, the carbon pores are populated by cations and anions, and a high initial molar strength (>50 mM) results in the 1:1 exchange of co-ions (ions with the same charge as the electrode) and counterions (oppositely charged ions), while maintaining the total number of ions within a pore. The ion distribution and population in porous carbon electrodes depend strongly on the presence of polar surface functional groups[18]. Charge is stored but only through non-permselective ion exchange, which does not contribute towards the depletion of ions in the electrolyte between the electrodes. The permselectivity can be enhanced by the use of polymeric or ceramic ion-exchange membranes (known as membrane CDI)[19–21], but the problem of co-ion expulsion can only be partially addressed[22–24]. CDI cells can also use carbon suspensions as the electrodes, enabling continuous desalination[25–28].

To overcome the limitations of desalination through carbon-based ion electrosorption, the CDI community has started exploring different electrochemical processes (FIG. 1). Thus, the immobilization of ions is no longer limited to physical electrosorption. Processes such as surface redox binding[29], ion insertion[30–35], conversion reactions[34–36] or charge compensation with redox-active electrolytes[37,38] are characterized by charge transfer across the fluid–solid interface between the electrolyte and electrode, and can be leveraged for water remediation. This research direction was pioneered in 2012, with the report of a desalination battery that operates through Na^+ insertion into a $Na_{2-x}Mn_5O_{10}$ electrode and the Ag/AgCl conversion reaction[39]. This work demonstrated that charge-transfer materials can operate in aqueous media with a high ionic concentration, enabling electrochemical seawater desalination — a concentration domain usually inaccessible with conventional CDI based on nanoporous carbon materials. Subsequently, various electrode materials have been adopted for desalination, many having been originally explored in the context of energy storage[40]. These reversible electrochemical-desalination techniques are not limited to water desalination[41] and have been extended to a range of water-remediation applications[41], including the removal of heavy metals[42–45], nutrient ions[46,47] and valuable elements (especially lithium)[48–54]; water softening[55]; ion separation[45,53,54,56,57] and water disinfection[52,58–60]. The dependency of electrochemical processes on concentration gradients and temperature can also be used for energy harvesting (also known as blue energy or capacitive mixing)[61–65]. Moreover, harnessing low-grade thermal waste energy from, for example, cooling towers is a promising route towards sustainable electrochemical processes for environmental applications[66].

In this Review, we first introduce suitable performance metrics and cell architectures for electrochemical desalination. We then discuss the mechanisms for ion removal by electrochemical processes, namely, ion electrosorption, ion insertion (or intercalation), conversion reactions and the charge compensation of redox electrolytes.

Electrochemical-desalination metrics

Ion-removal capacity, efficiency and rate

For electrochemical desalination, the charge at the electrodes is compensated by the ionic charge of cations and anions. Consequently, the amount of salt (ions) removed (immobilized) from a feed-water stream depends on the invested charge of the electrode, and it is convenient to normalize the desalination capacity to the electrode mass rather than the area of the electrode or, if present, membrane[67]. This rationale also explains the continued use of the term CDI, with capacitive meaning to have a capacity or behave like a capacitor[68]. Given that many different electrochemical processes are available, we instead refer to the technology as electrochemical desalination. The invested charge can be reported in farads, the unit of capacitance, only for capacitors or capacitor-like systems (pseudocapacitors); when redox reactions or other charge-transfer processes occur, it is preferential to quantify the invested and recovered charges in mAh (or mAh g^{-1})[69,70].

Salt-adsorption capacity is one of the most common performance metrics for evaluating electrochemical-desalination technologies. Gravimetric salt-adsorption capacity is based on the mass of salt (typically, NaCl) removed per mass of electrode, yielding a unit of $mg_{salt}\,g^{-1}{}_{electrode}$ (REF.[71]). This metric is calculated by a recording the time integral of the difference between the cell inflow and effluent concentrations and multiplying by the flow rate through the cell:

$$\frac{Mv}{m}\int_{t_0}^{t_i} c\,dt \qquad (1)$$

Here, v is the flow rate (l min^{-1}), $c\,dt$ is the salt concentration as a function of time (mol $min\,l^{-1}$), t_0 and t_i are the start and end times of the desalination process, respectively, M is the molecular mass of the salt and m is the mass of the electrode (g).

As desalination can also be accomplished by ion-insertion or electrochemical processes other than electrostatic adsorption, we suggest the use of the term desalination capacity instead of salt-adsorption capacity.

For systems with different ions[50,57,72], it is more reasonable to compare the molar amount of salt removed ($\mu mol_{salt}\,g^{-1}{}_{electrode}$) instead of the mass[73,74]. Moreover, when comparing electrode materials with very different molar masses, it may be more practical to normalize the desalination performance by the electrode

Author addresses

[1]INM – Leibniz Institute for New Materials, Saarbrücken, Germany.
[2]Department for Materials Science and Engineering, Saarland University, Saarbrücken, Germany.
[3]Department of Chemical and Biomolecular Engineering, University of Illinois at Urbana–Champaign, Urbana-Champaign, IL, USA.
[4]School of Chemical and Biological Engineering, College of Engineering, Institute of Chemical Process, Seoul National University, Seoul, Republic of Korea.
[5]Asian Institute for Energy, Environment & Sustainability, Seoul National University, Seoul, Republic of Korea.
[6]Korea Environment Institute, Sejong-si, Republic of Korea.
[7]Department of Chemistry and Bar-Ilan Institute of Nanotechnology and Advanced Materials, Bar-Ilan University, Ramat-Gan, Israel.

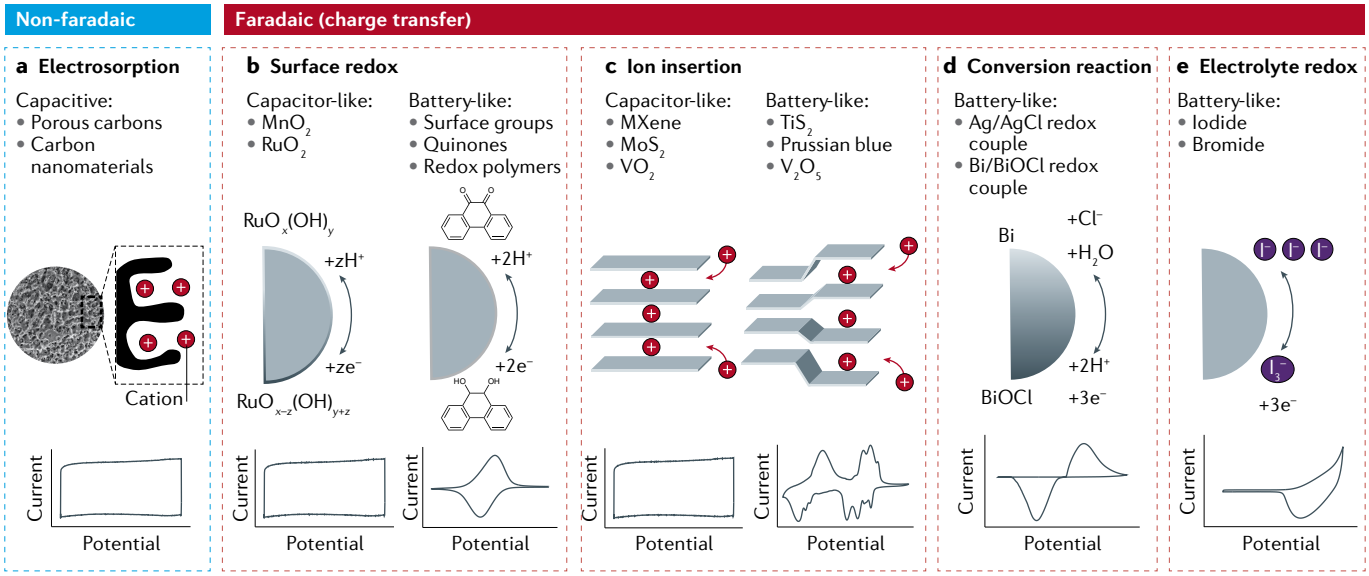

Fig. 1 | **Electrochemical processes for ion immobilization.** Ion immobilization can occur through non-faradaic (electrical double-layer) (panel **a**) or faradaic (charge-transfer) (panels **b**–**e**) processes. The latter include battery-like and capacitor-like redox reactions, as well as ion-insertion processes, conversion reactions and redox processes involving dissolved ions within the electrolyte (electrolyte redox)[263]. In all cases, ion removal is enabled by balancing the electric charge at an electrode surface, in an electrode material or in a (redox) electrolyte. The electrochemical signatures of the charge-storage mechanisms are seen in the cyclic voltammograms. Note that some of the surface redox processes shown are yet to be applied to electrochemical desalination and/or ion separation.

volume ($mg_{salt}\,cm^{-3}{}_{electrode}$)[75]. The only exception is redox electrolytes, for which the limiting factor is not the mass of the electrode but the charge of the dissolved redox-active ions[21,37,38]. In this case, it is practical to normalize to either the volume of the redox electrolyte or the area of the membrane that separates the redox electrolyte from the feed-water stream.

In addition to desalination capacity, it is equally important to quantify the amount of salt released during electrode regeneration. Under equilibrium conditions, equal amounts of salt are removed and released. Away from equilibrium, the two amounts may deviate, especially during the initial cycles of operation or in the presence of electrode-specific degradation processes. The ratio between the desalination capacity and release capacity is, therefore, an important diagnostic tool to understand electrode and system conditioning.

As desalination usually involves the bulk removal of cations and anions, desalination capacity relates to salt removal (that is, the removal of both cations and anions). However, when comparing, for example, ion-separation processes or exploring different electrode materials for the removal of either anions or cations, it is practical to quantify only the amount of removed cations or anions[76].

The efficiency of salt removal — or charge efficiency[10] — is defined as the ratio of the removed salt to the invested electric charge:

$$\frac{Fn_s}{Q_{charge}} \tag{2}$$

where F is the Faraday constant (26.801 Ah mol^{-1}), n_s is the number of moles of salt removed per half cycle and Q_{charge} is the total charge accrued during charging (Ah).

Ideally, the charge efficiency would approach unity, indicating that all the invested charges are used for ion removal. However, there are many factors that decrease charge efficiency, including cell resistance, surface redox reactions[77], co-ion expulsion[78], non-permselective ion exchange[78,79] and irreversible redox reactions[59,80]. When comparing different set-ups and cells, it is important to clarify whether the charge efficiency includes the charge lost per cell resistance (leakage current)[81].

The invested charge can also be analysed, enabling irreversible charge loss to be quantified; however, this does not necessarily translate to a difference between the ion-removal capacity and ion-release capacity. The coulombic efficiency quantifies the ratio of the discharge capacity to the charge capacity:

$$\frac{Q_{discharge}}{Q_{charge}} \tag{3}$$

where $Q_{discharge}$ (Ah) is the charge recovered during discharging.

In addition to the desalination capacity, it is also important to consider the rate at which desalination (or salinization during electrode regeneration) is accomplished, giving a metric in the units of $mg\,g^{-1}\,s^{-1}$ or $mol\,g^{-1}\,s^{-1}$:

$$\frac{\frac{Mv}{m}\int_{t_0}^{t_i} c\,dt}{t} \tag{4}$$

Unlike desalination capacity, which can be considered an equilibrium value, the desalination rate depends greatly on the intrinsic kinetics of the electrode materials, electrode engineering (including packing density and

thickness), cell engineering (for example, cell architecture and flow-channel design) and operational parameters (such as flow rate and charge–discharge rate)[13,82]. Similar to the use of Ragone plots to compare the performance of energy-storage devices[83,84], the desalination rate can be plotted against the desalination capacity. The resulting Kim–Yoon plots (or CDI Ragone plots)[82] show the trade-off between the amount of removed salt and the corresponding rate; the desalination capacity converges to equilibrium at low desalination rates.

A less commonly used factor to quantify desalination efficiency is the flow efficiency[7], which is dependent on the residence time (time for an ion to travel through the cell) and the half-cycle time during desalination or salinization:

$$\frac{f - 2nLp}{2fT} \tag{5}$$

where f is the superficial velocity of the pore solution (cm s^{-1}), n is the number of interfaces between the electrodes in a stack (for example, $n = 5$ for a stack with six electrodes), L is the electrode thickness (cm), p is the porosity of the electrode and T is the half-cycle time (s). The flow efficiency is a suitable metric to assess the issue of ion flow; specifically, cyclic operation of a desalination cell requires feed water to flush the immobilized ions from the electrodes, and it is important to limit the amount of processed water relative to the amount of remediated water.

Water recovery more generally relates the volume of processed water, $V_{processed}$, to the volume of desalinated water, $V_{desalinated}$, and is strongly dependent on the parameters of cell operation (that is, flow rate, flow-channel volume and half-cycle time):

$$\frac{V_{desalinated}}{V_{processed}} \tag{6}$$

Selectivity metrics

Increasing the selectivity of electrochemical separations is of growing interest, owing to the economic and environmental benefits of removing toxic or valuable species, and the associated energetic benefits of removing only the ions of concern[85]. Through the functionalization of carbon[86] or the implementation of redox-active processes[87], electrochemical interfaces and materials that can select target ions are an achievable goal. Thus, together with the advances in materials chemistry, there is a growing need to establish standardized selectivity metrics for quantifying ion separations. The separation factor is a standard metric for quantifying selectivity in chemical separations[88]. For a binary system of molecular species (A and B), the separation factor, $S_{A/B}$, for an adsorption process can be defined as:

$$\frac{[c_A / c_B]_{solid\ phase}}{[c_A / c_B]_{liquid\ phase}} \tag{7}$$

in which the concentrations of A and B (c_A and c_B, respectively) are the final equilibrium values after adsorption contact. The numerator can often be expressed in terms of the adsorption uptakes, q_A and q_B, of the species, which are obtained from adsorption-isotherm studies. In the case of binary adsorption of two cations, species A could be, for example, Na^+, and species B, K^+. Creating an electrode with a high separation factor becomes important for the up-concentration of valuable elements or the removal of micropollutants. Compared with carbon-based materials, charge-transfer adsorbents have higher separation factors, owing to their intercalation and redox-binding desalination mechanisms (described below). The separation factor has been used as a metric to quantify the selectivity of redox-polymer-based electrodes for the electrosorption of certain anions, including carboxylates and oxyanions, over competing anions in the electrolyte[45,73], as well as the selective removal of caesium from hazardous waste using hexacyanoferrate electrodes[89]. We expect that selectivity metrics will be increasingly and more rigorously implemented, allowing for easier cross-material and cross-process comparison of the performance of electrochemical-desalination systems for selective ion removal.

Energy metrics

Evaluating the energy consumption of electrochemical desalination is key to the development of energy-efficient technologies, especially for enabling comparison with other water-remediation methods[24,90,91]. Unlike traditional separation processes, electrochemical-desalination systems can (partially) recover the invested energy during discharge. The simplest metric for evaluating the energy consumption is the specific energy consumption, which is the total energy spent to remove a certain amount of salt (often specified in J mol^{-1} or J mg^{-1})[15,90,92]. The specific energy consumption can be evaluated using either the total input energy or the net energy consumed (calculated by subtracting the energy recovered during the discharge step), depending on the mode of operation[91]. The specific energy consumption varies dramatically according to the degree of energy recovery[93], operation mode (constant voltage vs constant current)[90], concentration of the solution, cell design and water recovery. Thus, a full understanding of the system requires the parameterization of the specific energy consumption under various operating modes to determine the optimum parameter space. The invested desalination energy (also known as the energy-normalized adsorbed salt) in units of moles of salt per joule of energy lost is given by[91]:

$$\frac{\nu}{E_{in} - E_{out}} \int_{t_0}^{t_i} (c_0 - c)\mathrm{d}t \tag{8}$$

where E_{in} and E_{out} are the energy invested during charging and energy recovered during discharging, respectively, and c_0 is the feed concentration. By evaluating energy metrics at various voltages and currents, the limitations of these electrochemical technologies can be identified and improved[94]. For example, evaluation of the constant-current and constant-voltage modes under different operating conditions reveals that, when

discharging at a constant voltage of 0 V, no energy is recovered, whereas discharging at constant current results in partial energy recovery. In parallel, thermodynamic energy efficiency is a metric that incorporates thermodynamic considerations with the energy consumption and is defined as the ratio of the Gibbs free energy of separation to the specific energy consumption[90]. This ratio represents the fraction of energy consumed during electrochemical desalination compared with that of an ideal thermodynamically reversible process to achieve the same level of separation.

In analogy to electrochemical energy-storage devices[95], the performance of desalination cells and the associated energy metrics are typically normalized to the electrode mass or volume of full or half cells to enable the comparison of materials and processes.

Scalability

Although not the focus of this Review, we note the growing importance and attention being devoted to techno-economic and feasibility analyses of electrochemical-desalination systems. A global sensitivity analysis was conducted for different electrochemical-desalination technologies to explore which parameters, including applied current density, influent concentration, electrode and system resistance, and electrode porosity, influence performance metrics[96,97], such as salt-adsorption capacity, average salt-adsorption rate and energy recovery. According to this analysis, the desalination capacity, charge efficiency and thermodynamic efficiency of membrane CDI were higher than those of traditional CDI and flowable electrode CDI. Device-level benchmarking can be used to assess the applicability of electrode materials, processes and associated cell designs for scaled, industrial applications[97]. For example, the trade-off between capital and operating costs was studied in a recent techno-economic analysis using a parameterized process model; this analysis highlighted the importance of decreasing capital costs, especially for membrane CDI, for which the cost of the ion-exchange membranes is high[98]. The lifetime of the electrodes dictates the feasibility and the relative advantages of CDI or membrane CDI over other water-purification technologies, with an important challenge being the preservation of electrode stability over multiple cycles[98]. Increasing the lifetime and decreasing the cost are, thus, key considerations in the development of synthetic materials for redox-active and faradaic adsorbents. The thermodynamic efficiency of electrochemical-desalination technologies has also been evaluated[99], providing insight into sources of inefficiency, as well as the effect of inlet concentration, water-recovery ratio and salt-removal ratio, among other factors, on the thermodynamic efficiency[100].

Despite progress in desalination capacity, desalination rate and energy analysis, it remains a challenge to deconvolute the influence of cell design and operational parameters on performance from the intrinsic ability of electrode materials or electrochemical processes to accomplish desalination. This applies not only to bulk energetic considerations but also, and even more so, to desalination rates[82]. Therefore, it is important to define the boundary conditions for benchmarking energy metrics.

Cell design

Electrochemical desalination relies on the permselective and/or non-permselective processes of the electrode materials and, if applicable, on the properties of the membrane (with or without ion-exchange ability). One can differentiate between one-channel, two-channel and three-channel desalination cells, which may or may not include an ion-exchange or porous membrane. Although cell designs with more than three flow channels are possible, the electrochemical desalination gradually transitions towards a concept closer to electrodialysis and, thus, are not discussed further here[101]. Rather than focusing on the geometry of the feed-water stream with respect to the electrodes (that is, flow-by, flow-through or flow-with)[71], we classify the cell designs according to the number of flow channels (FIG. 2); this classification is mechanism-agnostic and applies equally to electrosorption and/or charge-transfer processes.

The one-channel cell design is typically used in conventional CDI (FIG. 2a). Adding one cation-exchange or anion-exchange membrane or a pair of ion-exchange membranes to a one-channel cell (FIG. 2b) increases the desalination performance by enabling (or enhancing) permselectivity.

When using a pair of electrodes to remove (and release) solely cations or anions, desalination can be accomplished using a two-channel design with either an anion-exchange membrane or a cation-exchange membrane (FIG. 2c,d). This cell configuration is also known as rocking-chair desalination[33] or, depending on the target ion, sodium-ion desalination[31,101] (FIG. 2c) or chloride-ion desalination[35,102,103] (FIG. 2d). During charge–discharge of the cell, the target ion (for example, Na^+ in the case of sodium-ion desalination) is immobilized by one electrode, while being concurrently released on the other side. Owing to the use of an ion-exchange membrane, the oppositely charged ions (Cl^- in the case of sodium-ion desalination) must serve as agents for charge compensation and migrate from the target-ion uptake channel to the target-ion release channel. In this way, one effluent stream is depleted of ions, while the other is enriched.

A three-channel design features a pair of ion-exchange membranes for the selection of oppositely charged ions (FIG. 2e) or, often used with suspension electrodes (FIG. 2f), a pair of porous separators[104]. Thereby, the inflow and outflow is decoupled from the side channels. The static-electrode, three-channel cell (FIG. 2e) enables control over the local chemical environment at each electrode; thus, the ion concentration can be modified in the non-flow reservoirs or the electrolyte changed by using a different solvent. For example, a bi-electrolyte cell that features a non-flow side channel with the organic solvent propylene carbonate was developed to extend the operational cell voltage and increase the desalination capacity[105]. The side channels may also host a redox-active electrolyte, such as an iodide-containing or bromide-containing electrolyte[21,37]. However, the gradual loss of redox-active ions

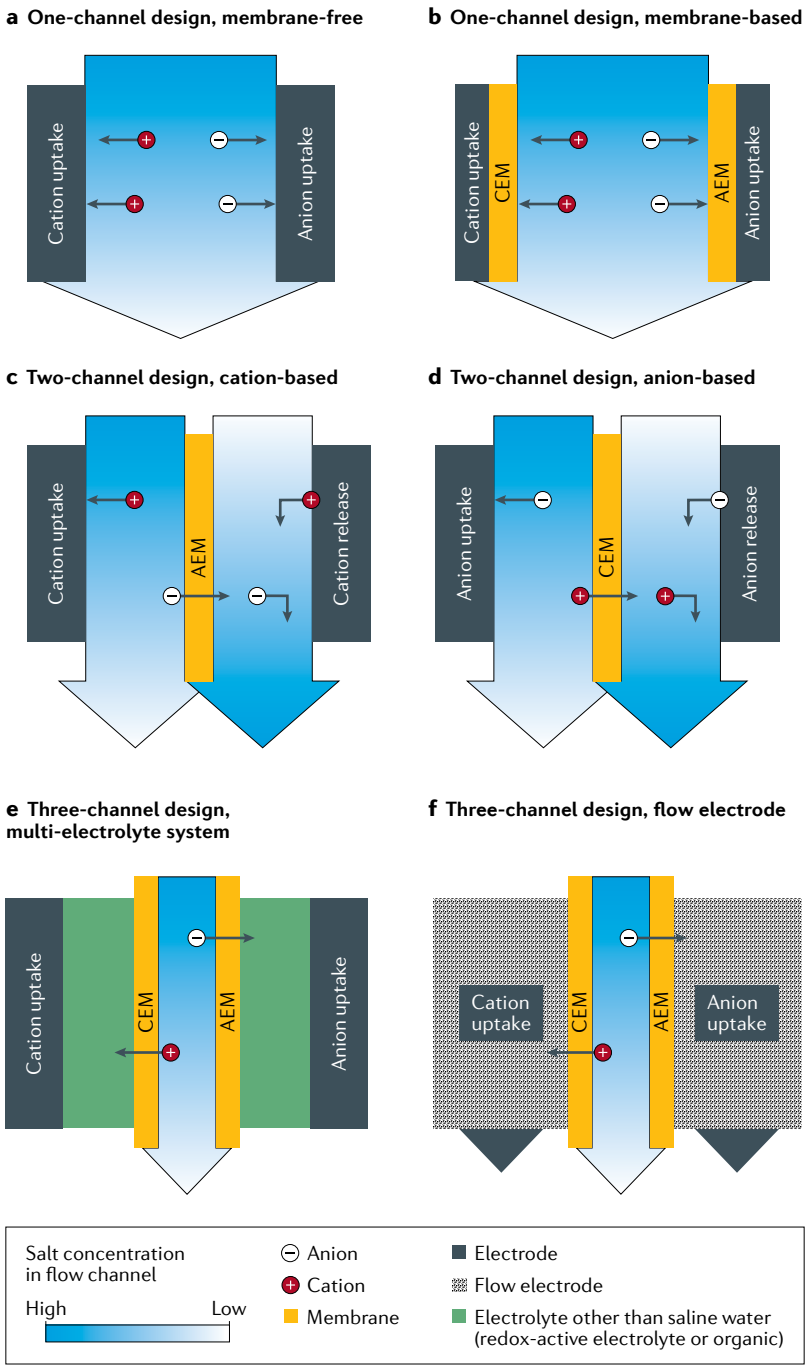

Fig. 2 | **Desalination cell designs.** Illustration of the main desalination cell types according to the number of channels. The electrode materials can undergo non-faradaic or faradaic (charge-transfer) processes and be static or flowable. The permselectivity can be increased by introducing additional channels separated by ion-exchange membranes or porous separators. AEM, anion-exchange membrane; CEM, cation-exchange membrane. Adapted from REF.[71], CC-BY-3.0 (https://creativecommons.org/licenses/by/3.0/).

across the membrane into the effluent stream is an issue for redox electrolytes. The desalination performance, thus, degrades over time and, depending on the identity of the redox-active ion, leaching may be an issue for potable-water generation[38]. Ion leaching can, however, be prevented by the use of advanced membranes, such as ceramic ones[21]. Flowable electrodes, separated by either porous separators or ion-exchange membranes, can also be used with a three-channel set-up. These electrodes are composed of a suspension of carbon particles and/or charge-transfer materials[25–28]. The high viscosity and granular convection of the suspension electrodes limits their application, prompting the implementation of an adapted fluidized-bed reactor design as an alternative[106].

Three-channel designs enable continuous desalination, as the suspension electrode or redox electrolyte can be regenerated in a second cell and fed back into the first one[26,37,107]. Continuous operation can also be implemented with a single module by circulating charged species between side channels, although this approach may require an additional ion-exchange membrane[108,109].

There is a complex relationship between cell design, cell operation and the resulting desalination performance, making a comparison of different electrodes materials (and pairings thereof) difficult. Electrode design is important to consider when analysing electrode pairs because the desalination kinetics is controlled by electrochemical processes and/or diffusion rates from the bulk electrolyte to the solid–liquid interfaces; this becomes more crucial at the system level, which may include arrays of electrodes pairs and multiple modules.

When comparing the performance of cells, the electrochemical-stability window of the electrolyte and electrode material must also be considered. In any cell configuration, the operational cell voltage should not exceed the electrochemically stable potential window to prevent parasitic water splitting (which does not contribute to ion removal) consuming charge and decreasing the energy efficiency[110]. The theoretical potential-difference limit for water is 1.23 V, but the value varies greatly, depending on the properties of the local fluid–solid interface, reactivity of the electrode materials, ionic strength and pH of the inflow. These factors can shift the hydrogen-evolution reaction and oxygen-evolution reaction below or above the theoretical potential. Moreover, when using electrode materials with different charge capacities, the two electrodes must be mass balanced to increase performance stability[111,112]. If the mass ratio of the electrode is not well balanced, the electrode with higher capacity may cause water splitting or other irreversible reactions.

Electrochemical-desalination mechanisms

Electrochemical-desalination mechanisms include electrostatic ion immobilization (conventional CDI), ion binding at redox-active surfaces, ion uptake through insertion processes or conversion reactions, and ion removal by charge compensation of redox-active polymers and redox-active electrolytes (FIG. 1). The variation in charge-storage mechanisms is reflected in the electrochemical signatures of the charge–discharge behaviour — capacitor-like or non-capacitor-like (battery-like) — as seen, for example, in the shape of the cyclic voltammograms (FIG. 1). Although the direct comparison of the desalination performance of different systems is difficult, for all systems, the invested electric charge correlates with the amount of removed salt, very much in the traditional sense of CDI.

Ion electrosorption

Desalination by ion electrosorption (FIG. 1a) is linked to the quantitative change in the ion concentration within the pores of the electrode materials. Numerous carbon materials have been explored for CDI[113], including activated carbons[114], carbide-derived carbons[115], graphene[116], carbon nanotubes[117], metal–organic-framework-derived carbons[118] and biomass-derived carbons[119]. However, ion electrosorption is not limited to carbon materials and can occur in other porous materials, such as metal–organic frameworks (providing electron transport is sufficiently enabled)[120].

To achieve ion permselectivity, open porous networks require the addition of an ion-exchange membrane or the design of a charge-transfer process. In the absence of permselectivity, electric charge within the porous network (for example, activated carbon) is compensated by the concurrent release of co-ions and immobilization of counterions. If co-ions are released, the charge efficiency of the system falls below 100% and may even fail to afford practical desalination, as occurs when concentrations exceed ~100–200 mM.

In the initial (uncharged) state (FIG. 3a), it can be assumed that the micropores of the electrode material contain an equal number of anions and cations. In response to an electrical charge at the pore wall, this balance is shifted by one of several modes: exclusive co-ion expulsion, leading to an increase in salinity; exclusive counterion uptake, lowering the salinity; or 1:1 non-permselective ion exchange, leaving the salinity unchanged (FIG. 3a). In the presence of anions and cations, charge storage within carbon nanopores is initially accomplished by ion exchange[79]. Once the reservoir of co-ions within the pores has been depleted, the system transitions towards counterion electrosorption[17] (FIG. 3b). At high molar strength, the large number of co-ions may preclude the system from achieving significant desalination capacity within the electrochemical-stability window of water (FIG. 3c). In low-concentration brackish water, the non-permselective ion-exchange regime dominates only at the lowest state of charge (FIG. 3d), and the influence of this detrimental regime can be decreased by not fully discharging the electrodes (that is, cycling between a cell voltage of, for example, 0.2–1.2 V)[121].

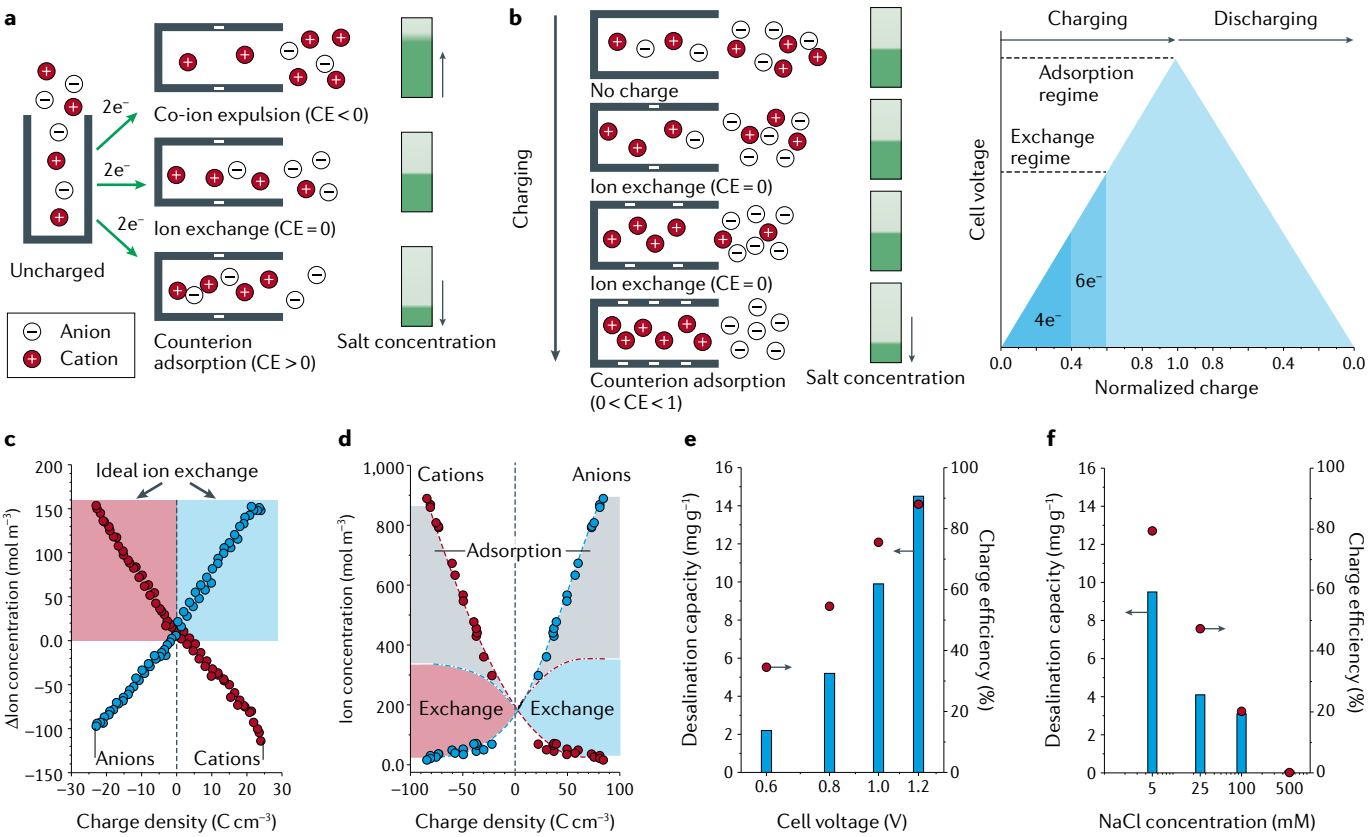

Fig. 3 | **Ion electrosorption. a** | In the absence of permselectivity, an electric charge in the electrode can be compensated by co-ion expulsion (increasing the salt concentration), counterion adsorption (decreasing the salt concentration) or ion exchange (no change in salt concentration). **b** | At sufficiently low molar strengths, a continuously charged nanopore will first undergo ion exchange before entering the permselective counterion-removal domain, leading to a decrease in salt concentration. The graph shows the transition from ion swapping to counterion absorption as a function of the cell voltage and invested charge. **c**,**d** | Plots showing the in-pore ion concentration with respect to the applied electronic charge at 1 M (panel **c**) and 20 mM (panel **d**) NaCl concentrations. The non-permselective ion-exchange regime dominates at 1 M, whereas, at 20 mM, the system transitions to permselective counterion adsorption once the in-pore population of co-ions has been depleted. Data from REFS[14,79]. **e**,**f** | Plots showing the effect of cell voltage (panel **e**) and salt concentration (panel **f**) on the desalination capacity and charge efficiency (CE). Data for panel **f** from REFS[188,264]. Panels **a** and **b** adapted from REF.[71], CC-BY-3.0 (https://creativecommons.org/licenses/by/3.0/). Panel **c**, data from REF.[79]. Panel **d**, data from REF.[14]. Panel **e** adapted with permission from REF.[264], Elsevier. Panel **f**, data from REF.[188].

The presence of charged functional groups on the electrode surface can favourably shift the point of zero charge to enhance the desalination performance[77,78,122]. In this way, the surface of carbon can be tailored to fully invert the CDI process, such that desalination is accomplished during discharging of the electrodes and regeneration during charging[123].

For an ideal nanoporous electrode, the cell voltage should be maximized to ensure facile electrosorption if water splitting is thermodynamically feasible. A higher cell voltage not only enables a larger desalination capacity but also increases the charge efficiency (FIG. 3e). By contrast, increasing the salt concentration causes a severe drop in the ability to desalinate an aqueous[124] or organic medium[124]. For example, the desalination capacity of activated carbon at a salt concentration of 5 mM is ~10 mg g^{-1} at a cell voltage of 0.8 V but drops to 4 mg g^{-1} at 25 mM, and above 100 mM, no meaningful desalination is possible (FIG. 3f). However, upon decreasing the pore size to ~1 nm, uncharged carbon nanopores become ionophilic[125,126], enabling CDI at high molar strengths, albeit at a lower charge efficiency. For example, at a NaCl concentration of 800 mM, activated carbon cloth with an average pore size of 0.59 nm achieved a desalination capacity of ~5 mg g^{-1} with a charge efficiency of ~30% at a cell voltage of 1 V (REF.[126]).

The addition of permselective ion-exchange membranes helps to overcome these intrinsic limitations of nanopores, enabling seawater desalination[127]. Ion-exchange membranes also extend the voltage window of cell operation from, for example, charging at +1.2 V and discharging at 0 V to discharging at −1.2 V. Without an ion-exchange membrane, reversal in the cell voltage leads to a mirroring of the initial ion-immobilization process, with no benefit to the desalination process. With ion-exchange membranes, the mode of charge compensation is limited to permselective counterion electroadsorption and, thus, inversion of the cell voltage can double the desalination capacity[128–130].

Even with ion-exchange membranes and voltage inversion, the desalination capacity of carbon electrodes is limited by the limited charge-storage capacity of carbon materials. For conventional CDI, typical values are in the range 10–30 mg g^{-1} (REFS[131,132]) (TABLE 1), but values of up to 20–60 mg g^{-1} are possible with membranes and higher salt concentrations[128]. The charge-storage limitation of carbon materials and the influence of quantum capacitance have been intensely investigated[133,134]. The ability to screen an ionic charge depends on the electronic structure of the carbon material. Modifying the degree of crystalline ordering[135] or heteroatom doping[136] are two common ways to increase the interfacial capacitance of carbon electrodes. For example, pyridinic and pyrrolic nitrogen-doped graphene exhibits a desalination capacity of 4.8 mg g^{-1}, whereas non-modified graphene delivers a desalination capacity of 3.8 mg g^{-1} (REF.[137]).

Table 1 | **Performance of selected electrochemical-desalination mechanisms and materials**

Mechanism	Material or redox couple	Cell design and features	Desalination capacity (mg g^{-1})	Charge efficiency (%)	Refs
EDLC	Activated porous carbon	–	3–27	>70[a]	13,47,188,212,244–251
Insertion	1D metal oxides ($Na_{0.44}MnO_2$, tunnel MnO_2)	–	6–68	>90	4,30,39,172,209
	2D metal oxides (MnO_2, hydrated V_2O_5)	–	9–37	>80	74,76,252,253
	2D TMDs (TiS_2, MoS_2)	–	9–25	>90	57,162,188
	2D MXenes (Ti_3C_2, $Mo_{1.33}C$)	–	13–45	>90	32,75,184
	2D metal phosphates ($Na_xVOPO_4{\cdot}yH_2O$)	–	24	58	178
	3D Prussian blue analogues (NiHFC, NaFeHFC, $K_{0.03}Cu(FeCN_6)_{0.65}{\cdot}0.43H_2O$)	–	32–130	35–96	33,199,254–259
	3D NASICON ($Na_2FeP_2O_7$, $NaTi_3(PO_4)_3$, $Na_3V_2(PO_4)_3$)	–	30–140	>90	161,211,212,260–262
Conversion	Ag/AgCl	One channel or two channel with a coupling electrode (e.g. carbon, $Na_3V_2(PO_4)_3$–rGO, $NaTi_3(PO_4)_3$ or $Na_{0.44}MnO_2$)	17–115	>90	35,209–212
	Bi/BiOCl	One channel with a coupling electrode (e.g. $Na_{0.44}MnO_2$, $NaTi_2(PO_4)_3$)	>68	>90	4,36
Redox electrolyte	EDLC/NaI	Porous carbon electrode with an AEM and CEM, or AEM and NASICON	20–80	87	21,38
	$ZnCl_2$/NaBr	Graphite electrode with an AEM and CEM	–	98[b]	37
	$ZnCl_2/K_4FeCN_6$	Graphite electrode with an AEM and CEM	–	85[b]	217
	$Na_4Fe(CN)_6{\cdot}10H_2O$	Porous carbon electrode with an AEM and CEM	68	>90	219

AEM, anion-exchange membrane; CEM, cation-exchange membrane; EDLC, electric double-layer capacitor; HFC, hexacyanoferrate; NASICON, sodium superionic conductor; rGO, reduced graphene oxide; TMD, transition-metal dichalcogenide. [a]Up to a salt concentration of 100 mM. [b]Percentage of salt removed.

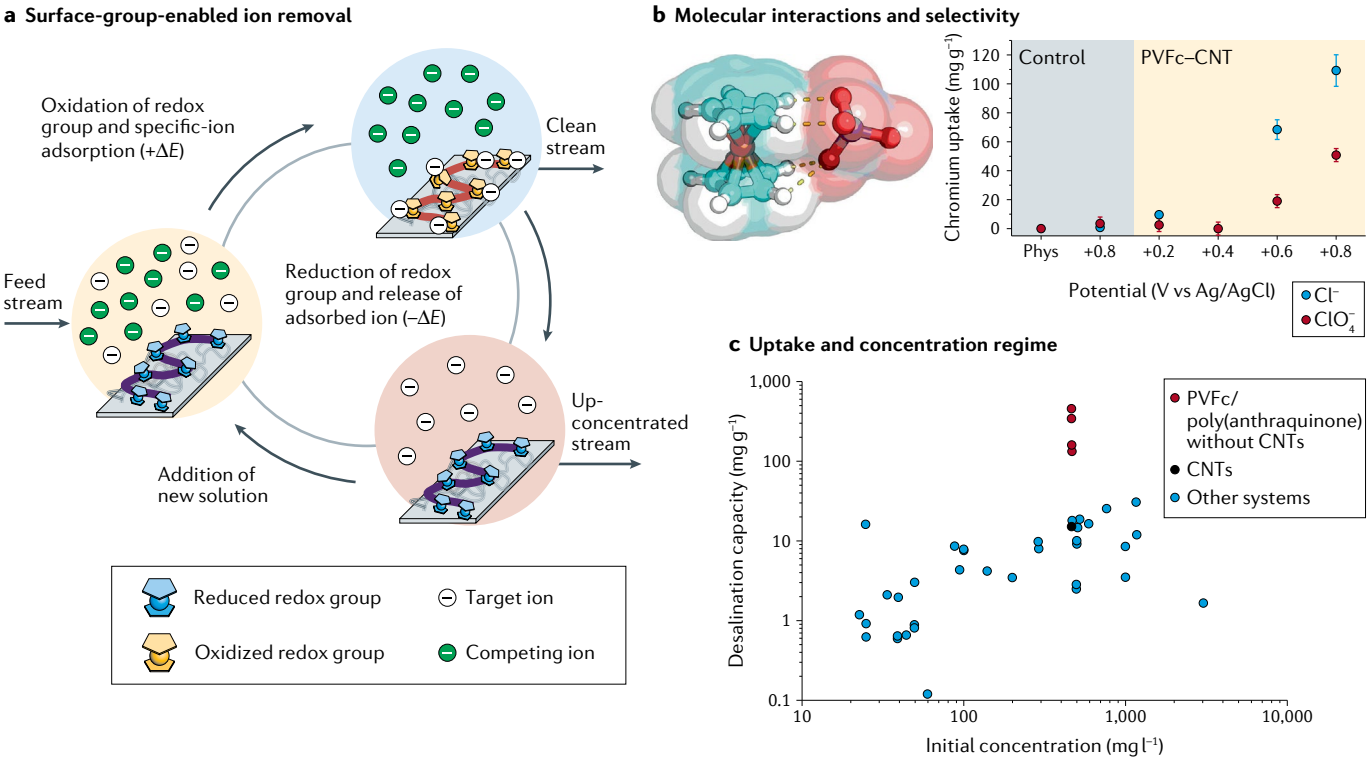

Fig. 4 | **Redox-active polymers. a** | Illustration showing the concept of selective ion removal through the reversible electrochemical reactions of tailored surface groups. Δ*E* is the change in the electrode potential. **b** | Poly(vinyl)ferrocene (PVFc) has good selectivity for various anions and can strongly bind electron-donating species, such as oxyanions (left part). The plot (right part) compares the uptake of chromium oxyanions by carbon nanotube (CNT) and PVFc-modified CNT (PVFc–CNT) electrodes at different potentials from solutions containing competing anions (Cl^- or ClO_4^-). The 'Phys' data point indicates the uptake when no potential is applied. The error bars represent the standard deviation from three measurements. **c** | Comparison of the ion-uptake capacity of various redox-functionalized electrodes (red) over a range of initial concentrations with those for CNTs (black) and other capacitive-deionization systems (blue). Panel **a** adapted with permission from REF.[73], Wiley-VCH. Panel **b** adapted from REF.[45], CC-BY-4.0 (https://creativecommons.org/licenses/by/4.0/). Panel **c** adapted with permission from REF.[146], ACS.

Furthermore, sodium removal has been demonstrated using pyridinic and pyrrolic nitrogen[138]. However, the redox activity of such groups may also be detrimental to the performance; for example, nitrogen-doped and sulfur-doped biomass-derived carbons showed lower charge efficiencies than those without heteroatoms.

Another issue is the electrochemical degradation of carbon electrodes in saline media with high concentrations of dissolved oxygen; the reduction of dissolved oxygen at the cathode yields corrosive hydrogen peroxide, which causes a gradual loss in performance[59,139]. These issues can be addressed by the use of a cation-exchange membrane to confine the peroxide anions or by modifying the oxygen-reduction reaction at the carbon surface by introducing a catalytically active material, such as titanium dioxide[140]. Nevertheless, to further increase the desalination capacity and eliminate the need for ion-exchange membranes for the remediation of saline media with high ionic strength, alternative electrode materials and desalination mechanisms have been demonstrated[40,141].

Redox-active polymers

Redox-active and conducting polymers are promising materials for electrochemical desalination (FIG. 1b), especially for selective ion separation: conducting polymers enhance the selectivity of electrodes towards target ions and improve their effectiveness for deionization by increasing the conductivity and presenting charged surface groups. Electroactive polymers have traditionally been studied in various sensing[142], energy-storage[143] and memristor[144] applications. Discrete electron transfer from the current collector to the backbone or side chain of a polymer modulates the affinity of an electrode surface towards charged, and even uncharged, species (FIG. 4). In many cases, charge injection or withdrawal dramatically affects the ion selectivity of the electrode by either activating specific interactions or changing macroscopic properties. Through judicious design, modulation of the ion–electrode interaction can increase the salt-removal capacity and selectivity for specific ions.

Organometallic redox polymers are particularly promising for controlling surface electrosorption. For example, poly(vinyl)ferrocene (PVFc) is a versatile and robust system for controlling charge-transfer interactions with several target anions, ranging from organic anions to transition-metal oxyanions (FIG. 4a). The interaction between the ferrocene units and various anions has been closely studied in sensing applications[145]. PVFc-coated electrodes have a strong affinity towards carboxylates, sulfonates and phosphonates over other

anions[73]. When properly coupled with a counter electrode, redox-active polymers can suppress side reactions and selectively capture micropollutants present in even trace amounts[29]. For example, reducible cobalt-based organometallic polymers have an affinity for cations and also serve as efficient cathodes[29]. PVFc-based electrodes have been used for the capture of heavy-metal oxyanions (FIG. 4b), demonstrating uptake capacities of >50 mg g^{-1} for chromium and arsenic oxyanions in an electrolyte with a 20-fold excess of competing anions and >90% removal at ppb concentrations in a waste-water matrix[45]. Furthermore, in a comparison of their ion uptake, selective PVFc electrodes showed a much higher electrosorption performance than state-of-the-art CDI technologies[146] (FIG. 4c). Recently, the combination of PVFc and a nitroxide radical polymer (poly(TEMPO methacrylate)) enabled the selective capture of toxic As(III) and conversion to the less harmful As(V), with >90% removal efficiency and electrocatalytic-conversion efficiency[147]. PVFc selectively adsorbs As(III) with high selectivity over Cl^- and, upon release, the poly(TEMPO methacrylate) on the counter electrode promotes the conversion of As(III) into As(V).

Polypyrrole and polyaniline are other examples of redox-active and conducting polymers that have been used for redox-driven ion electrosorption[148,149]. For example, functionalization of the polyaniline backbone with thiol groups enables efficient mercury adsorption[150]. Thiol-functionalized polyaniline adsorbs mercury at concentrations as low as 1–10 ppm; the Hg^{2+} ions can be regenerated by applying a reverse potential[150]. Selective capture is not limited to charged species: the macroscopic properties of redox-active molecules and polymers, including hydrophobicity, can be electrochemically modulated to enable the affinity for neutral species to be reversibly switched. For example, the conformation and, thus, hydrophobicity of a surfactant-functionalized conducting polypyrrole can be electrochemically switched to enable the reversible adsorbance and release of neutral compounds[151]. Polypyrrole was shown to be an effective electrode material for chloride storage within a seawater-desalination battery, which demonstrated a stable energy storage and NaCl-storage capacity over 200 cycles[152]. Similarly, polyelectrolyte-coated electrodes can enhance the desalination performance, as the charged functional groups along the polymer backbone increase counterion adsorption[153].

For many redox-active polymers, control of the binding mechanism can be enhanced by understanding the mechanism for ion interaction. For example, the cyclopentadienyl groups of PVFc preferentially bind to strongly electron-donating species, such as oxyanions and organic contaminants, through a combination of electrostatics and hydrogen bonding[45,73] (FIG. 4b, left). As for other classes of charge-transfer materials, optimization of the design of the electrochemical cell can also strongly increase the ion selectivity[154].

We expect interest in electroactive polymers and their application in water purification to grow, owing to their ease of processing and immobilization, as well as the ability to synthetically tune the selectivity. Moreover, alternative redox-active materials have begun to be explored for electrochemical desalination. For example, a cathode based on a redox-active covalent organic framework (COF) was developed for NaCl removal. When used in a single-flow-channel configuration with a COF-derived carbon anode, the system achieved a desalination capacity of 23 mg g^{-1} in 8.5-mM NaCl solutions using a cell voltage of 1.6 V (REF.[155]). The introduction of new COFs[156] could lead to increased application of these materials in water desalination.

Ion insertion

Water desalination through ion insertion (or intercalation) involves the insertion of a cation or an anion into a specific or non-specific interstitial site of the electrode materials[157] (FIG. 1c). Insertion materials are usually crystalline and highly ordered, but less ordered structures or amorphous materials can also reversibly host inserted ions[158,159]. Most insertion materials can host cations (for example, Li^+, Na^+ and K^+) and some (such as MXenes) can host both anions and cations. Depending on the volume expansion and structural reversibility, more spacious interstitial sites yield increased cyclic stability, larger ion-storage capacity (higher charge-storage capacity) and faster kinetics (that is, ion diffusion in the host material)[160]. The electrochemical current versus potential signature of insertion materials can vary greatly, ranging from a pseudocapacitive signature for insertion into non-specific sites (for example, in many-layer materials) to a battery-like plateau for insertion into specific sites (such as in $Na_2FeP_2O_7$ or the rhombohedral (1T) phase of TiS_2)[161,162].

There are various ways to categorize ion-insertion materials based on, for example, their chemical composition or crystal-structure features. Another way to differentiate ion-insertion materials is to consider the dimensionality of the insertion sites (FIG. 5a). One-dimensional insertion materials show a tunnel-like structure with channels for ion transport, resulting from the connections between metal–oxygen polyhedra, such as in $Na_{0.44}MnO_2$ (REFS[163,164]) or connections between phosphate tetrahedra and metal–oxygen polyhedra, such as in $LiFePO_4$ (REFS[165,166]). Two-dimensional insertion materials can be layered, with examples including polyanionic phosphates (hydrous and anhydrous), transition-metal carbides, transition-metal oxides and transition-metal dichalcogenides (TMDs)[167]. These materials accommodate inserted ions between the in-plane layers. Three-dimensional insertion structures, such as inorganic framework materials (for example, Prussian blue) or sodium superionic conductor (NASICON)-type materials, have an open framework or cage-like structure into which ions can be inserted from all directions and possess large spacings for ion accommodation[168].

One-dimensional insertion materials. One-dimensional insertion materials were the first to be implemented for electrochemical desalination[39]. For example, $Na_{0.44}MnO_2$, which has an orthorhombic crystal structure with 2 × 2 and 1 × 3 tunnels occupied by Na^+, can uptake Na^+ but has no ability to insert Cl^-. Following sodiation, the cyclic voltammogram shows several

broad redox peaks, which combine pseudocapacitive and battery-like features[169] (FIG. 5b, left). With a charge capacity of 35 mAh g^{-1} (REFS[39,170]), $Na_{0.44}MnO_2$ has a theoretical sodium-removal capacity of 15 mg g^{-1}, which corresponds to a NaCl-normalized desalination capacity of 38 mg g^{-1}. An all-$Na_{0.44}MnO_2$ device with a two-channel design has been demonstrated, comprising two $Na_{0.44}MnO_2$ electrodes with different sodium contents[31]. By coupling the 1D insertion material with other electrode materials (for example, activated porous carbon, Ag, AgCl and BiOCl), the desalination capacity varies between 6 and 68 mg g^{-1} (TABLE 1).

Within the manganese-oxide family, there are many tailorable tunnel structures built from vertex-sharing and edge-sharing MnO_6 octahedra[171]. These materials possess different tunnel sizes and shapes, and can provide a large crystallographic volume for accommodating ions, including larger ions such as K^+ and Mg^{2+}, which are important for water-softening applications[172]. For example, although hollandite MnO_2 and todorokite MnO_2 have similar structures, the tunnels are wider in the latter[172]. By altering the synthesis method, the number of subunit octahedra can be controlled, enabling the tunnel size to be increased. The wide tunnels are typically

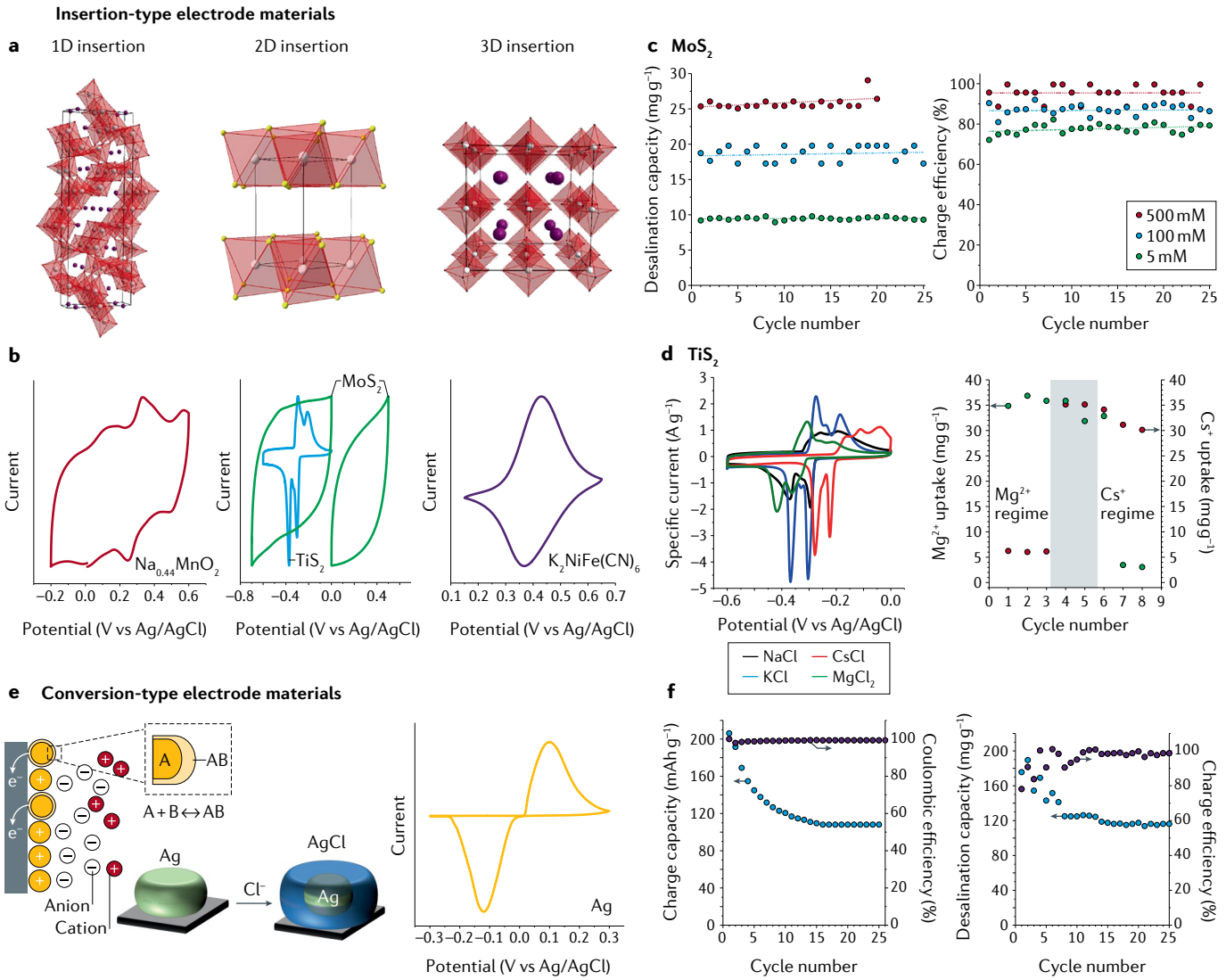

Fig. 5 | **Ion-insertion and ion-conversion reactions. a**,**b** | Ion-insertion materials can be categorized according to the dimensionality of the intercalation site (panel **a**). These materials show different electrochemical responses, as revealed in the corresponding cyclic voltammograms (panel **b**). **c** | The electrochemical-desalination performance (in terms of desalination capacity and charge efficiency) of hexagonal close-packed MoS_2 (2H-MoS_2), a typical 2D layered material, in different concentrations of aqueous NaCl (REF.[188]). **d** | Two-dimensional layered TiS_2 demonstrates selective ion removal. The left part shows the cyclic voltammograms of rhombohedral-phase (1T)-TiS_2 in different electrolytes. The right part shows the uptake of Mg^{2+} and Cs^+ by 1T-TiS_2 from a mixed-cation system[57]. By changing the electrode potential, it is possible to switch from a Mg^{2+}-uptake regime (−396 to −220 mV vs Ag/AgCl) to a Cs^+-uptake regime (−219 to 26 mV vs Ag/AgCl). The grey region corresponds to a regime (−396 to −160 mV vs Ag/AgCl) that shows only weak selectivity for Mg^{2+} over Cs^+. **e** | Schematic showing the process of desalination through conversion reactions, as exemplified for the Ag/AgCl reaction. The cyclic voltammogram shows distinctive charge-transfer peaks. **f** | Plots showing the change in charge capacity, desalination capacity, coulombic efficiency and charge efficiency over time for a desalination cell based on the Ag/AgCl conversion reaction[35]. Panel **a** (left) and panel **b** (left and middle, TiS_2) adapted with permission from REF.[170], ACS. Panel **b** (middle, MoS_2) and panel **c** adapted with permission from REF.[188], RSC. Panel **d** adapted with permission from REF.[57], Wiley-VCH. Panel **e** (right) and panel **f** adapted from REF.[35], CC BY 3.0 (https://creativecommons.org/licenses/by/3.0).

filled with cations (such as Li^+, K^+ and Na^+) and/or water to maintain the structure. The electrochemical signature of tunnel-structured MnO_2 differs from that of $Na_{0.44}MnO_2$ and is pronouncedly pseudocapacitive[173].

Ferric phosphate with an olivine structure is capable of reversible cation insertion and is, accordingly, a known cathode material for sodium-ion batteries with a theoretical specific capacity of 110 mAh g^{-1} at the operational potential of 3 V versus Na/Na^+ (REF.[174]). More recently, an electrode made of a composite of amorphous $FePO_4$ and reduced graphene oxide was paired with a porous carbon electrode in a one-channel, membrane-based cell[159] (FIG. 2b). The device achieved a desalination capacity of 100 mg g^{-1} in 40-mM NaCl solutions when cycling the cell voltage between −1.4 V and +1.4 V (REF.[159]).

Two-dimensional insertion materials. Two-dimensional insertion materials include layered materials, such as metal carbides, nitrides and carbonitrides (MXenes)[175,176], TMDs[167], some metal oxides[76,177] and phosphates[178]. Many of these materials can intercalate cations and anions, but the ability to host certain ions depends on the specifics of the ion-insertion site (including the chemical environment, atomic spacing and kinetics to reach the site) and the ionic species[179,180].

First reported in 2011 (REF.[181]), MXenes are the most recent addition to the fast-growing family of 2D materials. MXenes have the general formula $M_{n+1}X_nT_x$ ($n = 1$, 2, 3), where M is an early transition metal, X represents carbon and/or nitrogen, and T_x is the surface termination functional group (usually fluoride or oxygen) with variable composition and stoichiometry (x). The physico-chemical and electrical properties of MXenes strongly depend on the type and number of surface groups[181–183]. The chemical structure of MXenes depends on the ternary metal carbides or nitrides (known as MAX phases, where A is a group 13 or 14 element) from which they are derived. The three main groups of ternary MAX (that is, the 211, 312 and 413 phases) produce MXenes of different layer thicknesses after etching[176]. Most MXenes show a hexagonal close-packed structure with more than one stacking order, that is, ABAB and ABCABC. The first MXene explored for water desalination was $Ti_3C_2T_x$, which reversibly intercalates Na^+ and Cl^- with a capacitance of 176 F g^{-1} and 84 F g^{-1} for negative and positive polarization, respectively[32]. Although MXenes enable cation and anion insertion, the negative charge of the oxygen and fluoride surface groups limits the desalination performance at the anion-removal electrode. At low salt concentration (5 mM), $Ti_3C_2T_x$ has a desalination capacity of 13–45 mg g^{-1}, depending on the synthesis conditions (TABLE 1). The MXene $Mo_{1.33}CT_x$, which has ordered divacancies and is produced from $(Mo_{2/3}Sc_{1/3})_2AlC$, has also been investigated for electrochemical desalination[184]. $Mo_{1.33}CT_x$ exhibits a specific capacitance of 150 F g^{-1} for both positive and negative polarization, which simplifies the charge balancing for a symmetric set-up. The resulting desalination capacity is ~15 mg g^{-1} at a cell voltage of 0.8 V for 600-mM aqueous NaCl solutions. For some MXenes, especially Ti-based ones, oxidation and hydrolysis (especially in oxygen-rich aqueous media) of the materials may limit the performance stability[185].

TMDs have a typical chemical formula of MX_2, where M is a transition metal and X is a chalcogen (S, Se or Te). M and X are covalently bonded in the plane, with one layer of metal atoms sandwiched between two layers of chalcogens. Each trilayer is held together by weak van der Waals forces, enabling exfoliation of these layers[186]. Multilayered TMDs adopt a hexagonal close-packed structure (the 2H phase). Once 2H-TMD domains are reduced to a thickness of a few layers, so-called nanoflakes, the properties notably change, particularly in regards to the ion-insertion capacity[187]. A few-layer 2H-MoS_2 obtained through electrochemical activation showed both anion and cation intercalation with a pseudocapacitive response (FIG. 5b, centre) and a specific capacitance of 200 F g^{-1} for negative and positive polarization[188]. Thin-layered MoS_2 has been effective for water desalination over a wide range of salt concentrations (FIG. 5c). The desalination capacity and charge efficiency increase with the salt concentration, which is in contrast to the performance of porous carbons. Many TMDs also exhibit a rhombohedral structure (the 1T phase). The advantage of the 1T phase is that it is a metal-like conductor with a narrow bandgap energy[189,190]. 1T-TiS_2 is cation selective and exhibits two distinct pairs of redox peaks in the cyclic voltammogram (FIG. 5b, centre), owing to intercalation in, first, every other layer (corresponding to the first peaks) and, subsequently, all remaining layers (corresponding to the second peaks), with the cations occupying the octahedral and trigonal prismatic sites[191]. With a maximum charge capacity of 70 mAh g^{-1}, the measured sodium-uptake capacity of 1T-TiS_2 is in the range 30–40 mg g^{-1}, depending on the initial sodium-ion concentration[162]. The inability of TiS_2 to host anions allows for the design of a one-channel desalination cell without an ion-exchange membrane, using activated carbon cloth as the counter electrode; the resulting pair provides a desalination capacity of 15 mg g^{-1} at a charge efficiency of >70%, even at high (600-mM) NaCl concentrations[162]. The strong shift in intercalation potential for different cations also enables materials such as TiS_2 to be used in separations. Alkali-metal ions have different numbers of water molecules in their hydration shells, resulting in a variation in the desolvation energy during ion intercalation[170]. Consequently, the intercalation potential of TiS_2 shifts according to the cation present in solution (FIG. 5d, left), enabling the intercalation of a specific ion by choosing a suitable electrode potential (FIG. 5d, right). Layered metal oxides are mostly found as dioxides, trioxides and pentoxides (for example, MnO_2, MoO_3 and V_2O_5, respectively)[192–194]. In the context of water desalination, V_2O_5 and MnO_2 have been investigated (TABLE 1). Orthorhombic hydrated vanadium pentoxide (h-V_2O_5) is composed of layers of trigonal bipyramidal polyhedra with water interlayers[195]. h-V_2O_5 shows a cation-insertion-type pseudocapacitive response with a desalination capacity of 24 mg g^{-1} (REF.[76]) in 600 mM NaCl with a cell voltage between −0.4 V and 0.8 V. Birnessite MnO_2 has a hexagonal structure composed of edge-sharing MnO_6 octahedra. Similar to h-V_2O_5, birnessite MnO_2 accommodates Na^+ between the layers, resulting in a desalination capacity of 9–37 mg g^{-1} (TABLE 1).

The interlayer ions or water influence the ion-removal performance, as they affect the interlayer spacing[74]. For example, Mg-birnessite MnO_2 with Mg^{2+} in the interlayer can be synthesized by ion exchange of Na^+ in Na-birnessite MnO_2 with Mg^{2+}. Mg-birnessite MnO_2 exhibits a larger interlayer spacing than that in Na-birnessite MnO_2, resulting in a higher desalination capacity (37 mg g^{-1}) compared with that of Na-birnessite MnO_2 (31 mg g^{-1})[172].

Vanadyl phosphate ($VOPO_4$) has a structure similar to that of NASICON, with VO_6 octahedra connected to four PO_4 tetrahedra instead of six PO_4 units. Depending on their orientation and the edge-sharing between VO_6 and PO_4, the resulting structure can be tetragonal or orthorhombic[196]. To maintain the layered structure, vanadyl phosphate requires interlayer water or intercalant alkali-metal ions (for example, Li^+ or Na^+). After the intercalation–deintercalation or exfoliation process, $Na_xVOPO_4{\cdot}yH_2O$ undergoes a phase change (forming, for example, $VOHPO_4$ or $VOPO_4{\cdot}xH_2O$), owing to the loss of interlayer water or cations, resulting in an increase in the desalination capacity[178,197]. In aqueous media, the electrochemical response of hydrated vanadyl phosphate is battery-like, with a charge capacity of ~35 mg g^{-1}, which corresponds to a desalination capacity of 24 mg g^{-1} (TABLE 1).

Three-dimensional insertion materials. Three-dimensional insertion materials explored for electrochemical water treatment and ion separation so far fall into two categories: Prussian blue and its analogues, and NASICON-type materials. Prussian blue, $A_xFe[Fe(CN)_6]{\cdot}zH_2O$ (where A is an alkali metal) has an open 3D organometallic-like framework that adopts a face-centred cubic structure (FIG. 5a, right). The framework comprises low-spin Fe^{2+} and high-spin Fe^{3+} coordinated to the carbon and nitrogen of the cyanide anions, respectively. The interstitial sites are usually occupied by alkali-metal ions (for example, Na^+ or K^+) and/or water, depending on the preparation conditions. Various Prussian blue analogues have been explored. For example, a nickel analogue, $A_xNiFe(CN)_6$, can be prepared by replacing Fe^{2+} with Ni^{2+}. More complex analogues can be prepared by replacing both Fe^{2+} and Fe^{3+} with other transition metals. For example, $Mn_3[Co(CN)_6]_2{\cdot}nH_2O$ is produced by reacting $K_3[Co(CN)_6]_2$ with $Mn(CH_3COO)_2{\cdot}4H_2O$ (REF.[44]). Prussian blue and its analogues show battery-like electrochemical signatures (FIG. 5b, right), with the position of the redox peaks determined by the redox activity of the metals within the framework[198]. Thus, the chosen transition metal determines the redox potential.

To date, mostly Prussian blue analogues have been applied in electrochemical water treatment (TABLE 1). Depending on the cell design and the selected electrodes, Prussian blue analogues show a desalination capacity in the range 32–130 mg g^{-1}. The desalination capacity, desalination rate and cyclic stability of a multichannel cell (FIG. 2e) comprising a Prussian blue electrode coupled to Ag can be increased by altering the electrolyte concentration in the side channel. With a NaCl concentration of 10 mM in the feed stream and 1 M NaCl in the side channel, the system delivers a desalination capacity of up to 53 mg g^{-1}, which is approximately twofold higher than with 10 mM NaCl in the side channel[199].

NASICONs, with the general formula $A_xMM'(XO_4)_3$ (where A is an alkali metal, M and M′ are transition metals and X is P, Mo, W or S), are highly crystalline materials with large interstitial spaces. The basic structure consists of two MO_6 octahedra sharing all corners with XO_4 tetrahedra, resulting in a rhombohedral crystal structure. The redox potential of NASICONs can be tuned by altering the anion or metal[196]. The best explored NASICON materials for water desalination are polyanionic phosphates ($A_xMM'(PO_4)_3$), owing to the high sodium-ion capacities (up to 3 mole per mole of NASICON)[200,201]. NASICONs exhibit selectivity for Na^+ over other cations, enabling a desalination capacity of 30–140 mg g^{-1} (TABLE 1).

Challenges for ion insertion in real conditions. Ion-insertion materials have several advantages over carbon materials, particularly for the desalination of high-salt-concentration feeds. However, in real water streams, the presence of natural organic matter is almost inevitable. The long-term impact of such substances in the feed water on electrode materials in electrochemical-desalination processes may be detrimental and remains poorly investigated.

Efforts have been made to determine the extent to which natural organic matter blocks the access of ions to the insertion (or deinsertion) sites of porous electrodes and how to regenerate polluted electrodes; however, the longevity has been increased only with low concentrations of dissolved organic matter[202–204]. In one example, $Na_{0.44}MnO_2$ electrodes in electrochemical-desalination cells were progressively deactivated, owing to the presence of a small amount of humic acid (200 mg l^{-1}) in a 200-mM NaCl feed solution[205]. The capacity-fading mechanism was attributed to the blockage of Na^+-insertion sites at the interface of the $Na_{0.44}MnO_2$ electrodes. Furthermore, the number of available binding sites for Na^+ decreased because of dissolution of manganese ions, promoted by the humic acid in the feed solution. This case exemplifies the major problems that may result from the presence of natural organic matter in electrochemical-desalination cells with inorganic intercalation electrodes, namely, surface passivation, as well as dissolution of transition-metal ions from the electrodes (either through ion exchange with protons or complexation of the transition-metal ions in solution), which affect long-term electrode stability[206]. As insertion materials usually have a small outer surface area compared with that of nanoporous carbons, they may be more susceptible to fouling.

Conversion reactions

Materials that undergo conversion reactions (FIG. 1d) transform into a new phase from the atomic constituents[157] (FIG. 5e, left). These materials have high specific charge capacities and, thus, deliver high desalination capacities. Using a suitable two-channel cell with anion-specific conversion-type materials, bulk removal of the anions is achieved through conversion reactions,

while the cations are removed through charge balancing. To date, only two conversion-type materials, both anion-specific, have been explored for electrochemical desalination, namely, Ag and Bi. Cation-specific conversion-type materials have yet to be explored, in part, owing to the challenge of identifying materials that undergo the necessary reactions within the limited stability window of water and the limited stability of these materials in water.

The Ag/AgCl redox couple is the best known conversion-reaction material in aqueous media and is frequently used as a reference electrode[207]. Upon oxidation, Cl^- reacts with bulk Ag, forming AgCl. For Ag/AgCl, this process produces a distinct one-electron transfer peak in cyclic voltammograms (FIG. 5e, right). Bismuth, by contrast, stores Cl^- through conversion to BiOCl:

$$Bi + Cl^- + H_2O \leftrightarrow BiOCl + 2H^+ + 3e^- \quad (9)$$

Considering the molar mass of BiOCl, the corresponding theoretical capacity of the BiOCl system is 103 mAh g^{-1}. For comparison, the theoretical capacity of the Ag/AgCl system is 248 mAh g^{-1} (normalized to the mass of Ag). The standard potentials of Bi/BiOCl and Ag/AgCl are 0.16 V and 0.22 V versus the standard hydrogen electrode[36], respectively. When used in desalination, the higher redox potential of the Ag/AgCl couple results in higher energy consumption. Nevertheless, Ag/AgCl and Bi/BiOCl have several similarities: selectivity towards Cl^- removal; the reactions of BiOCl and AgCl are kinetically slower than those of Bi and Ag, respectively; and the capacity retention quickly decays, owing to volume expansion (225% for Ag and 158% for Bi) during the conversion process[35,36].

To accomplish desalination, a chloride-selective electrode can be coupled with another electrode for cation removal, such as $Na_{0.44}MnO_2$, $NaTi_2(PO_4)_3$, $Na_3V_2(PO_4)_3$ or, simply, porous carbon[4,39,208–212] (FIG. 1a). When BiOCl was paired with $NaTi_2(PO_4)_3$ in a one-channel configuration, a desalination capacity of ~69 mg g^{-1} was achieved at a small cell voltage of 200 mV (REF.[36]). Owing to the involvement of H^+ in the discharge mechanism (Eq. 9), the discharge kinetics are highly dependent on the pH of the feed water. Acidic solutions decrease the overpotential required for BiOCl reduction but are not favourable for the desodiation of $NaTi_2(PO_4)_3$. Thus, the cell was redesigned and, after charging in salty water, the BiOCl and $NaTi_2(PO_4)_3$ electrodes were discharged separately in 70-mM HCl and 1-M Na_2SO_4 solutions, respectively, using an ion-exchange membrane[36].

When conversion materials are used together with insertion materials in a one-channel configuration, desalination capacities of up to 108 mg g^{-1} can be reached over a wide range of salt concentrations, but especially for high salt concentrations (510 mM)[39]. Alternatively, the same materials can be used in a two-channel cell configuration[34,35,213] (FIG. 2d) and, when combined with a cation-exchange membrane, invert the sodium-ion desalination (or rocking-chair) concept to yield a process that can be coined chloride-ion desalination[34,213]. A two-channel cell with Ag/AgCl electrodes achieved an initial desalination capacity of ~200 mg g^{-1} in 600 mM NaCl with a small operational voltage (200 mV), resulting in low energy consumption[35] (TABLE 1). This value is close to the theoretical desalination capacity (230 mg g^{-1}) of this material. However, conversion reactions are plagued by incomplete reversibility and grain coarsening, and, thus, the system performance may decrease through material instability[35] (FIG. 5f).

Redox-active electrolytes

The desalination concepts presented above all rely on ion removal by either electrosorption or faradaic reactions in bulk materials or at electroactive interfaces. Through modification of the cell architecture, electrochemical desalination can be accomplished even when only the cation or the anion participates in the process, because a two-channel system enforces bulk salt removal through charge compensation of the diluted stream. Charge compensation can also be applied for electrochemical desalination using a redox-active electrolyte (FIG. 1e), in which case, neither the removed anions nor cations are directly involved in the charge-transfer process. A redox-active ion (such as I^- or $[Fe(CN)_6]^{3-}$) dissolved in an electrolyte can change its oxidation state by accepting or donating electrons at the electrolyte–electrode interface (FIG. 6a). This redox activity is widely exploited in redox-flow batteries and redox-enabled supercapacitors[214]. Upon charging the electrode, the mobile redox-active anions diffuse close to the electrode interface and rapidly transfer an electron to the electrode[215]. Owing to the short diffusion-path length and the confinement of the redox-active ion within electrically conductive carbon nanopores, ion transport can be very fast and, in some cases, faster than conventional ion-electrosorption kinetics[214,216]. Subsequently, the oxidation state of the redox-active ion changes and these species may diffuse away from the solid–liquid interface. Redox-active electrolytes may provide a high charge-storage capacity (for example, 168 mAh g^{-1} for 1 M NaI), as the reactions typically involve the transfer of more than one electron[38].

A redox-active electrolyte can be used on one side of an electrochemical cell for the removal of Na^+ (FIG. 6a) and paired with a charge-transfer material or conventional nanoporous carbon electrode. It is also possible to have another redox-active electrolyte on the opposite side, and there are many possible pairings within the electrochemical-stability window of water (FIG. 6b). Thereby, the technology transitions fully into the field of redox-flow batteries[37,217,218].

In a recently proposed system, a redox-active electrolyte that undergoes a liquid–solid transition between dissolved zinc ions and metallic zinc was paired with a NaBr catholyte[37] (FIG. 6c). During charge and discharge, the charge neutrality in the redox-electrolyte compartments is maintained by the diffusion of Na^+ or Cl^- (or other ions for different salts) across ion-exchange membranes separating the feed-water stream. Such systems transition towards the concepts underlying electrodialysis cells. Alternatively, it is possible to pair two redox-active electrolytes with all oxidized and reduced species in a dissolved form. For example,

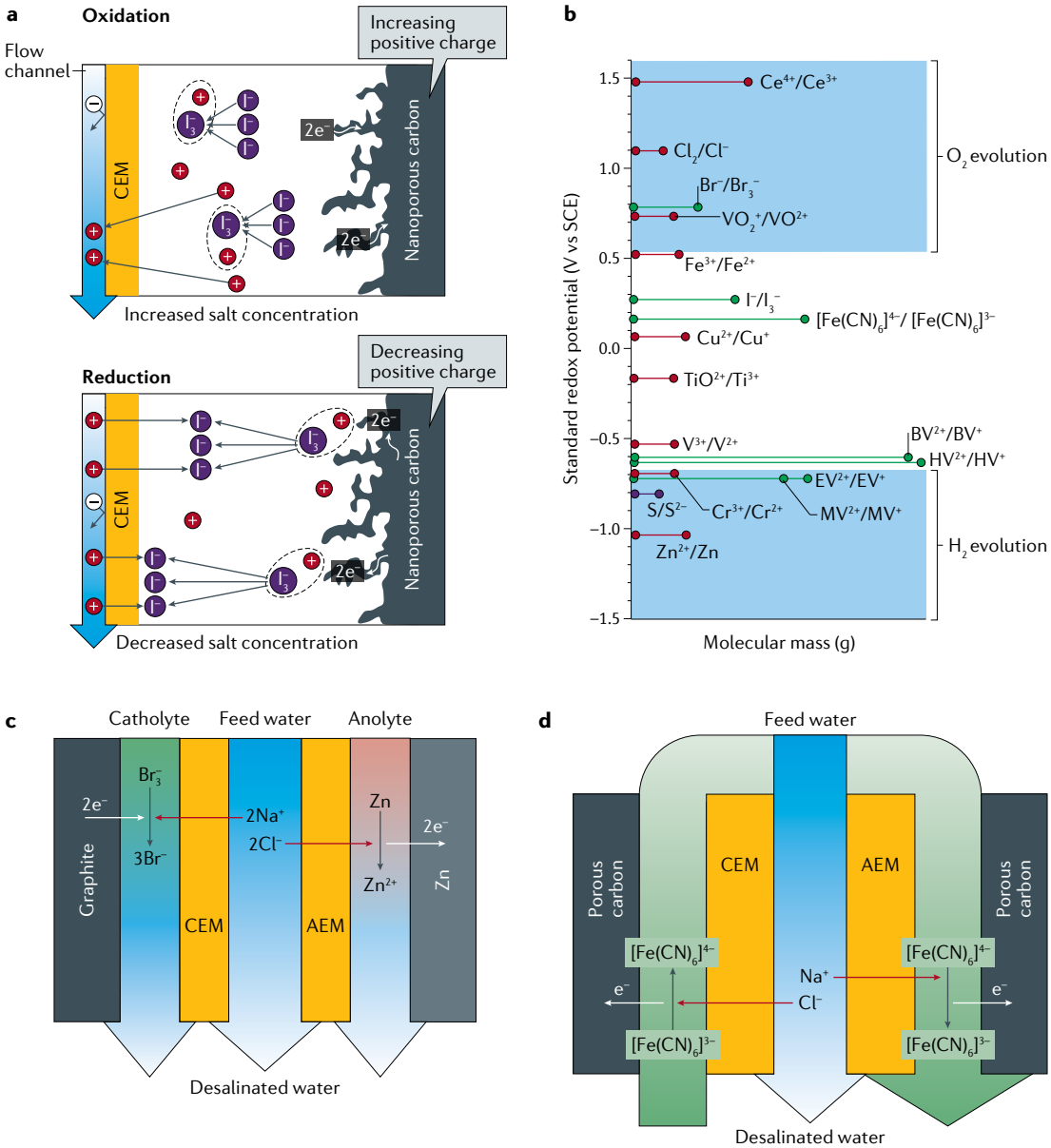

Fig. 6 | **Redox-active electrolytes. a** | Electrochemical-desalination mechanism with redox-active electrolytes. Following oxidation of I^- in the electrolyte to I_3^-, Na^+ ions are ejected through the cation-exchange membrane (CEM), resulting in the salinization of water in the effluent stream. In reverse, upon reduction of I_3^-, Na^+ ions migrate through the CEM to maintain charge neutrality in the electrolyte. Thereby, the effluent stream is desalinated. **b** | Reduction potentials (vs the standard calomel electrode (SCE)) of various catholyte and anolyte redox couples. Only redox couples with redox potentials within the electrochemical-stability window of water (white region) can be used in water desalination. The colours of the redox couples indicate stability in acidic (red), neutral (green) and basic (purple) electrolytes. **c**,**d** | Examples of multichannel desalination cells with redox-active electrolytes. AEM, anion-exchange membrane; BV, benzyl viologen; EV, ethyl viologen; HV, heptyl viologen; MV, methyl viologen. Panel **a** adapted with permission from REF.[21], ACS. Panel **b** adapted from REF.[265], CC-BY-4.0 (https://creativecommons.org/licenses/by/4.0/). Panel **d** adapted with permission from REF.[219], ACS.

a multichannel cell that uses a $[Fe(CN)_6]^{4-}/[Fe(CN)_6]^{3-}$ redox couple as both the catholyte and anolyte in the side channels (FIG. 6d) has been demonstrated for water desalination over a wide range of salt concentrations[219] (TABLE 1). Moreover, this concept enables fully continuous operation, much like with suspension electrodes, by recycling the oxidized and reduced redox electrolyte. Another example is the VCl_3/NaI redox system (Eqs. 10 and 11), for which desalination with an energy efficiency of 50% was demonstrated[218] with a cell voltage of 0.79 V.

$$VCl_3 + e^- \leftrightarrow VCl_2 + Cl^- \quad (10)$$

$$NaI_3 + 2Na^+ + 2e^- \leftrightarrow 3NaI \quad (11)$$

There are several challenges associated with the use of redox-active electrolytes. In assessing the performance

Table 2 | **Advantages and limitations of charge-transfer materials**

Type	Advantages	Disadvantages
Surface redox	Fast kinetics; high selectivity; good cyclability	Low charge capacity
Insertion (1D)	Good cyclability; moderate charge and desalination capacity	Mostly cation selective
Insertion (2D)	Good cyclability; moderate charge and desalination capacity; both cation and anion selective	Usually low electronic conductivity
Insertion (3D)	High charge and desalination performance; good cyclability	Usually low electronic conductivity
Conversion	High charge capacity; high desalination capacity	Low cycling stability; limited choice of materials
Redox electrolyte	High charge capacity; high desalination capacity; fast kinetics	Requires an ion-exchange membrane

of redox-active-electrolyte systems, it may not be useful to normalize the desalination performance to the mass of the solid charge-transfer electrode; instead, the performance should be normalized to the membrane area. However, this makes a direct comparison with CDI and other charge-transfer materials difficult because the desalination capacity for these systems is often reported in units of mg g^{-1}. Moreover, when using redox-active electrolytes, it is necessary to prevent the redox-active ions from shuttling between the two electrodes to avoid rapid self-discharge[220,221]. The redox-active ions must also be stopped from gradually diffusing into the effluent stream to avoid contamination and to maintain performance stability.

There are redox-active ions, such as Br^-, that could be environmentally harmful when released from an electrochemical desalination cell. However, a pair of porous-carbon electrodes in the set-up shown in FIG. 2a can exploit the different electro-oxidation potentials of Br^- versus, for example, Cl^- and water to selectively immobilize Br^- (REF.[222]). Similar trapping processes can be designed for other redox-active ions.

Electrode design and materials selection

The performance of charge-transfer materials and processes can exceed that of conventional carbon materials in terms of desalination capacity, efficiency, the variety of electrode pairings and suitability for different saline concentrations. However, the unambiguous comparison of these materials is impossible: only when tested under comparable conditions is it possible to establish comparative performance metrics, a problem that is well known in the energy-storage community[95]. Nevertheless, it is possible to identify some general advantages and disadvantages associated with the use of different classes of charge-transfer materials (TABLE 2).

Surface redox materials and redox electrolytes offer fast charge-transfer processes, which translates to fast desalination rates. However, thick electrodes may exhibit poor electron conductivity and, thus, lead to sluggish charge-transfer kinetics. Although surface redox processes can be used in desalination cells without ion-exchange membranes, electrodes should be paired such that one electrode is cation selective (for example, polypyrrole), while the other is anion selective (for example, PVFc).

Surface redox processes can have high ion selectivity, which can be beneficial for ion separation but detrimental when the goal is to achieve non-selective deionization of bulk water (such as saline media). Conversion-type electrode materials have a high desalination capacity; however, this enhanced charge-storage capacity is usually accomplished by processes with limited reversibility, and the performance may degrade (or the range of useable state-of-charge decrease) over time. Insertion materials, including 1D, 2D and 3D materials, have good cycling stability and moderate desalination capacities. Some 2D insertion materials, such as MXenes, can be used for both cation and anion removal, whereas other materials are typically selective towards one or the other.

Charge-transfer materials generally have lower conductivities than those of carbon materials and, thus, inevitably require carbon additives to optimize the charge capacity. However, achieving both fast charge transport and a high charge-storage capacity is a challenge; with too little carbon additive, the poor conductivity results in a low charge capacity, whereas too much carbon additive leads to a low faradaic contribution and, thus, low charge capacity. The type, amount and phase distribution of the conductive phase influences the charge-transfer kinetics, efficiency and overall performance stability. There is no governing rule on the mass loading of the carbon additives, but the goal is to optimize charge percolation on a micrometre and sub-micrometre level. Efficient charge percolation can be achieved by using conventional composite electrodes (that is, mechanical mixtures of a faradaic material and a conductive agent) or hybrid electrodes (that is, nanoscale, chemical binding between faradaic and carbon materials)[223,224]. Within the literature, the mass loading of carbon is ~7–30 mass% and the mass loading of the binder is ~5–10 mass%. The mass loading and phase of carbon should be optimized to maximize the mass loading of the active materials. However, the packing density of the active material, the type and amount of binder, and the fabrication of the electrode influence the resulting desalination metrics. For example, increasing the mass loading and density of the electrodes decreases the desalination rate[13,82].

Ion separations and heavy-metal removal

Charge-transfer materials not only show great promise for water desalination but also for applications requiring ion separation and selectivity, such as the removal of toxic ions and the recovery of valuable elements. The latter is of considerable interest, owing to the simplicity of the process (catch and release) and tunability compared with that of conventional separation processes (involving, for example, filtration, extraction, adsorption and crystallization)[41]. Some faradaic materials show an intrinsic preference towards a certain ion; for example, $LiFePO_4$ has a strong affinity for Li^+ and intercalates even trace amounts in the presence of a high concentration of Na^+ (REF.[225]). Another approach to selective ion removal is to exploit the different ion-intercalation potentials in multi-ion systems, whereby extrinsic ion selectivity is achieved by varying the applied cell voltage[57].

Given the growing importance of lithium-ion batteries[226,227], environmentally friendly and energy-efficient methods for lithium extraction are in high demand. Conventional lithium-extraction processes involve a series of time-consuming and costly precipitation steps[228]. Therefore, extracting lithium from seawater or sources with high lithium-ion concentrations, such as waste water from the mining industry or hydrothermal water, is an attractive alternative to conventional lithium mining[49,50,226,229,230].

Pioneering work on electrochemical lithium extraction[50,231] employed an intrinsically lithium-selective material ($LiFePO_4$) coupled with an exclusively chloride-selective electrode (Ag) and achieved a very high lithium recovery from a sodium-rich brine solution with low energy consumption (144 Wh kg^{-1}_{Li}). Follow-up studies have further demonstrated the effectiveness and energy efficiency of electrochemical lithium recovery[48,51]. For example, electrodes comprising spinel $LiMn_2O_4$ can selectively extract Li^+ from solutions that contain a high concentration of other ions (Na^+, K^+, Mg^{2+} and Ca^{2+}) with an energy consumption of 334 Wh kg^{-1} (REFS[48–50,226,230]).

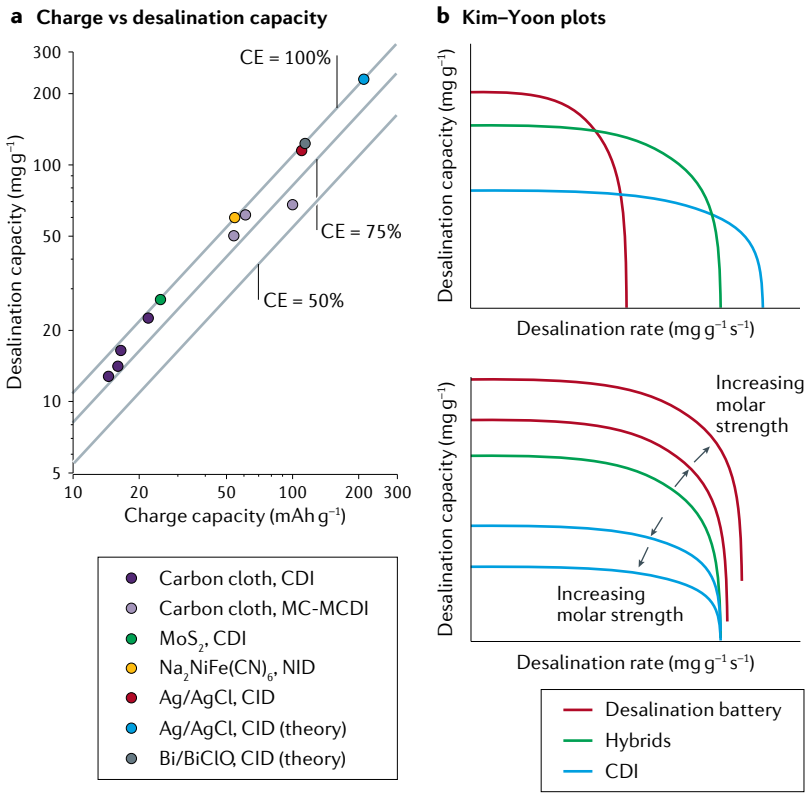

Fig. 7 | **Performance domains of electrochemical-desalination materials.** **a** | Correlation between the invested electric charge and resulting desalination capacity for selected carbon and non-carbon materials[35]. **b** | Ragone-like Kim–Yoon plots illustrate the domains of operation for fast desalination (through ion electrosorption) and high-capacity desalination (through charge-transfer materials; top part) and the influence of increasing molar strength on the performance metrics (bottom part)[82]. CDI, capacitive deionization; CE, charge efficiency; CID, chloride-ion desalination; MC-MCDI, multichannel membrane CDI; NID, sodium-ion desalination. Panel **a** adapted from REF.[35], CC-BY-3.0 (https://creativecommons.org/licenses/by/3.0/). Data for panel **b** from REF.[82].

Faradaic processes and materials can also be applied to recycle spent cathode materials. For example, a redox electrolyte ($[Fe(CN_6)]^{3-}/[Fe(CN_6)]^{4-}$) was used to extract lithium from spent $LiFePO_4$ (REF.[232]). Similar to redox-flow batteries, the cell consisted of a graphite felt cathode and anode, paired with a cation-exchange membrane. During operation, $[Fe(CN_6)]^{3-}$ selectively reacts with $LiFePO_4$ in the anolyte tank to form $[Fe(CN_6)]^{4-}$ and Li^+. As $[Fe(CN_6)]^{4-}$ flows into the cell, it is oxidized to $[Fe(CN_6)]^{3-}$, while Li^+ crosses the membrane and forms LiOH. Thus, lithium is selectively extracted as a high-purity salt with a removal efficiency of 99.8% (REF.[232]). The development of new lithium-selective materials and improved cell architectures will establish electrochemical lithium recovery as an important technology and, possibly, an alternative or supportive method for large-scale lithium production.

In the context of ion-separation processes, charge-transfer materials can also be applied to purify industrial products[41]. When using carbon electrodes, monovalent cations (such as Na^+ and K^+) are substituted by divalent cations (such as Ca^{2+} and Mg^{2+}), owing to the stronger electrostatic attraction[41]. Thus, carbon electrodes may have poor selectivity. Faradaic materials such as $Na_{0.44}MnO_2$ are Na^+ selective and intrinsically discriminate against competing cations (such as K^+, Mg^{2+} and Ca^{2+}). By pairing $Na_{0.44}MnO_2$ with a chloride-selective Ag electrode, the resulting cell delivers a Na^+ selectivity 13-fold higher than that for K^+ and 8-fold higher than that for Mg^{2+} and Ca^{2+} in 30-mM NaCl, KCl, $MgCl_2$ and $CaCl_2$ solutions; therefore, this system is attractive for KOH purification[53]. Replacing the Ag electrode with a Prussian blue ($K_xFe[Fe(CN)_6]$) electrode increases the K^+ concentration, owing to deinsertion of K^+ ions from the electrode, while Na^+ ions are removed by insertion into $Na_{0.44}MnO_2$ (REF.[54]). In a mixed-cation electrolyte (a solution containing 20 mM NaCl and 40 mM KCl), a cell with $K_xFe[Fe(CN)_6]$ and $Na_{0.44}MnO_2$ electrodes removed 36% of the Na^+ ions, resulting in a KCl purity of 99.8% (REF.[54]).

Environmental applications of electrochemical desalination specifically target the extraction of heavy metals, such as arsenic, cadmium, chromium and lead. So far, nanoporous carbons have mostly been explored for this task[233–239]. The pore size of carbon materials provides a degree of ion selectivity and enables the discrimination of ions based on their size and ionic charge[56,240]; thus, the hydration shell and associated desolvation energy are key aspects[241]. More recently, redox-active polymers have been investigated for the remediation of heavy metals, with PVFc selectively removing chromium and arsenic oxyanions from water at concentrations as low as 100 ppb (REF.[45]). Owing to the importance of the task and the need for molecular selectivity, we expect increased interest in redox-active electrodes for transition-metal separations.

Outlook

Having emerged as a promising technology for the remediation of brackish water and specialized industrial applications, electrochemical-desalination technologies have recently started to adopt charge-transfer materials.

In all cases, the main performance-limiting parameter is the correlation between the invested electric charge and the desalination capacity (FIG. 7a). The adoption of charge-transfer materials has enabled new applications, ranging from enhanced ion selectivity to direct desalination of highly concentrated saline media, including seawater. New cell concepts have also enabled continuous desalination operation, including designs that use suspension electrodes or redox-active electrolytes that are constantly replenished. Alternative concepts can even employ metal–air battery technology, as exemplified recently with zinc–air desalination[242]. Research on new electrode materials, cell designs and operation modes for various environmental and industrial applications continues. We foresee the consolidation of fast and high-capacity systems with different correlations between the desalination rate and capacity, depending on the ionic strength and desalination process (FIG. 7b). As the field matures, a clearer picture of the road map for electrochemical desalination will emerge and, ultimately, we may be able to create a library of materials, cells and operational parameters for the tailored design of desalination systems. However, realizing this goal will require comparable testing methods and metrics to be established and performance-stability testing over hundreds, if not thousands, of operational cycles.

Electrochemical desalination also offers opportunities to combine energy-storage and desalination processes. For example, units could be designed to serve as grid-scale buffers that use surplus electricity to produce potable water, but provide electrochemical energy by an inverse operation during periods of electricity shortage. Such concepts are ideally combined with photovoltaics or alternative renewable-energy sources.

Charge-transfer materials offer intrinsic advantages in terms of energy efficiency for electrochemical desalination. By combining high desalination capacity, low cell voltage and high reversibility, these materials enable low-energy, high-efficiency desalination. Optimal electrochemical desalination is achieved by using high-capacity electrode-material combinations that have a low voltage difference between them; this is in contrast to the optimal requirements for energy storage, for which high capacity and high cell voltage are desirable. Nevertheless, there are disadvantages of charge-transfer materials. For example, there are indications that the low external surface area of faradaic materials enhances their susceptibility to ageing and fouling[205,243]. Moreover, unlike other desalination techniques (for example, nanofiltration and reverse osmosis), electrochemical water desalination requires cyclic operation and regeneration of the electrodes. The latter can be overcome by either using flow electrodes composed of charge-transfer slurries or redox-active electrolytes. It also remains unclear how the costs of faradaic electrodes affect the techno-economic feasibility of charge-transfer-based desalination compared with that of conventional CDI based on nanoporous carbon.

Selectivity is now a major goal for electrochemical-desalination technologies, and charge-transfer materials have presented themselves as a prime platform for addressing these challenges. The design of electrode materials with bespoke and/or tunable ion selectivity could enable the targeted removal of pollutants, as well as the ability to up-concentrate precious elements, such as lithium or other metals, from seawater or mining waste water, providing new sources for raw materials. Studies of charge-transfer materials for desalination will also feed back into the energy-storage community by spurring the discovery of new reversible electrochemical processes and materials for technologies beyond lithium-ion batteries. Charge-transfer materials are, therefore, uniquely placed to provide a platform for sustainable electrochemical applications at the energy–water nexus.

Published online 22 April 2020

1. Werber, J. R., Osuji, C. O. & Elimelech, M. Materials for next-generation desalination and water purification membranes. *Nat. Rev. Mater.* **1**, 16018 (2016).
2. Ghaffour, N., Missimer, T. M. & Amy, G. L. Technical review and evaluation of the economics of water desalination: current and future challenges for better water supply sustainability. *Desalination* **309**, 197–207 (2013).
3. Jones, E., Qadir, M., van Vliet, M. T. H., Smakhtin, V. & Kang, S.-m. The state of desalination and brine production: a global outlook. *Sci. Total Environ.* **657**, 1343–1356 (2019).
4. Chen, F. et al. Dual-ions electrochemical deionization: a desalination generator. *Energy Environ. Sci.* **10**, 2081–2089 (2017).
5. Blair, J. W. & Murphy, G. W. in *Saline Water Conversion* Vol. 27 Ch. 20 (American Chemical Society, 1960). **First paper on electrochemical desalination, featuring a cell comprising a carbon electrode paired with Ag/AgCl**.
6. Murphy, G. W. & Caudle, D. D. Mathematical theory of electrochemical demineralization in flowing systems. *Electrochim. Acta* **12**, 1655–1664 (1967).
7. Johnson, A. M. & Newman, J. Desalting by means of porous carbon electrodes. *J. Electrochem. Soc.* **118**, 510–517 (1971).
8. de Levie, R. On porous electrodes in electrolyte solutions: I. Capacitance effects. *Electrochim. Acta* **8**, 751–780 (1963).
9. Bockris, J. O. M. The structure of water in the double layer. *Inorganica Chim. Acta* **40**, X14 (1980).
10. Zhao, R., Biesheuvel, P. M., Miedema, H., Bruning, H. & van der Wal, A. Charge efficiency: a functional tool to probe the double-layer structure inside of porous electrodes and application in the modeling of capacitive deionization. *J. Phys. Chem. Lett.* **1**, 205–210 (2009).
11. Evans, S. & Hamilton, W. S. The mechanism of demineralization at carbon electrodes. *J. Electrochem. Soc.* **113**, 1314–1319 (1966).
12. Biesheuvel, P. M., Fu, Y. & Bazant, M. Z. Diffuse charge and Faradaic reactions in porous electrodes. *Phys. Rev. E* **83**, 061507 (2011).
13. Porada, S. et al. Direct prediction of the desalination performance of porous carbon electrodes for capacitive deionization. *Energy Environ. Sci.* **6**, 3700–3712 (2013).
14. Porada, S., Zhao, R., van der Wal, A., Presser, V. & Biesheuvel, P. M. Review on the science and technology of water desalination by capacitive deionization. *Prog. Mater. Sci.* **58**, 1388–1442 (2013).
15. Dykstra, J. E., Porada, S., van der Wal, A. & Biesheuvel, P. M. Energy consumption in capacitive deionization - constant current versus constant voltage operation. *Water Res.* **143**, 367–375 (2018).
16. Beguin, F., Presser, V., Balducci, A. & Frackowiak, E. Carbons and electrolytes for advanced supercapacitors. *Adv. Mater.* **26**, 2219–2251 (2014).
17. Prehal, C., Koczwara, C., Amenitsch, H., Presser, V. & Paris, O. Salt concentration and charging velocity determine ion charge storage mechanism in nanoporous supercapacitors. *Nat. Commun.* **9**, 4145 (2018).
18. Rubin, S., Suss, M. E., Biesheuvel, P. M. & Bercovici, M. Induced-charge capacitive deionization: the electrokinetic response of a porous particle to an external electric field. *Phys. Rev. Lett.* **117**, 234502 (2016).
19. Biesheuvel, P. M. & van der Wal, A. Membrane capacitive deionization. *J. Membr. Sci.* **346**, 256–262 (2010).
20. Cho, Y. et al. A novel three-dimensional desalination system utilizing honeycomb-shaped lattice structures for flow-electrode capacitive deionization. *Energy Environ. Sci.* **10**, 1746–1750 (2017).
21. Lee, J. et al. High electrochemical seawater desalination performance enabled by an iodide redox electrolyte paired with a sodium superionic conductor. *ACS Sustain. Chem. Eng.* **7**, 10132–10142 (2019).
22. Kim, Y.-J. & Choi, J.-H. Enhanced desalination efficiency in capacitive deionization with an ion-selective membrane. *Sep. Purif. Technol.* **71**, 70–75 (2010).
23. Biesheuvel, P. M., Zhao, R., Porada, S. & van der Wal, A. Theory of membrane capacitive deionization including the effect of the electrode pore space. *J. Colloid Interface Sci.* **360**, 239–248 (2011).
24. Zhao, R., Porada, S., Biesheuvel, P. M. & van der Wal, A. Energy consumption in membrane capacitive deionization for different water recoveries and flow rates, and comparison with reverse osmosis. *Desalination* **330**, 35–41 (2013).
25. Jeon, S. I. et al. Desalination via a new membrane capacitive deionization process utilizing flow-electrodes. *Energy Environ. Sci.* **6**, 1471–1475 (2013).
26. Gendel, Y., Rommerskirchen, A. K. E., David, O. & Wessling, M. Batch mode and continuous desalination of water using flowing carbon deionization (FCDI)

technology. *Electrochem. Commun.* **46**, 152–156 (2014).
27. Hatzell, K. B. et al. Capacitive deionization concept based on suspension electrodes without ion exchange membranes. *Electrochem. Commun.* **43**, 18–21 (2014).
28. Porada, S. et al. Carbon flow electrodes for continuous operation of capacitive deionization and capacitive mixing energy generation. *J. Mater. Chem. A* **2**, 9313–9321 (2014).
29. Su, X. et al. Asymmetric Faradaic systems for selective electrochemical separations. *Energy Environ. Sci.* **10**, 1272–1283 (2017).
30. Lee, J., Kim, S., Kim, C. & Yoon, J. Hybrid capacitive deionization to enhance the desalination performance of capacitive techniques. *Energy Environ. Sci.* **7**, 3683–3689 (2014).
This study introduced the hybrid CDI concept.
31. Smith, K. C. & Dmello, R. Na-ion desalination (NID) enabled by Na-blocking membranes and symmetric Na-intercalation: porous-electrode modeling. *J. Electrochem. Soc.* **163**, A530–A539 (2016).
32. Srimuk, P. et al. MXene as a novel intercalation-type pseudocapacitive cathode and anode for capacitive deionization. *J. Mater. Chem. A* **4**, 18265–18271 (2016).
33. Lee, J., Kim, S. & Yoon, J. Rocking chair desalination battery based on Prussian blue electrodes. *ACS Omega* **2**, 1653–1659 (2017).
This paper presented rocking-chair desalination using Prussian blue.
34. Grygolowicz-Pawlak, E. et al. Coulometric sodium chloride removal system with Nafion membrane for seawater sample treatment. *Anal. Chem.* **84**, 6158–6165 (2012).
This paper introduced the chloride-ion-desalination concept.
35. Srimuk, P., Husmann, S. & Presser, V. Low voltage operation of a silver/silver chloride battery with high desalination capacity in seawater. *RSC Adv.* **9**, 14849–14858 (2019).
36. Nam, D.-H. & Choi, K.-S. Bismuth as a new chloride-storage electrode enabling the construction of a practical high capacity desalination battery. *J. Am. Chem. Soc.* **139**, 11055–11063 (2017).
37. Abu Khalla, S. & Suss, M. E. Desalination via chemical energy: an electrodialysis cell driven by spontaneous electrode reactions. *Desalination* **467**, 257–262 (2019).
38. Lee, J. et al. Confined redox reactions of iodide in carbon nanopores for fast and energy-efficient desalination of brackish water and seawater. *ChemSusChem* **11**, 3460–3472 (2018).
39. Pasta, M., Wessells, C. D., Cui, Y. & La Mantia, F. A desalination battery. *Nano Lett.* **12**, 839–843 (2012).
This study introduced the concept of the desalination battery.
40. Suss, M. E. & Presser, V. Water desalination with energy storage electrode materials. *Joule* **2**, 10–15 (2018).
41. Yoon, H., Lee, J., Kim, S. & Yoon, J. Review of concepts and applications of electrochemical ion separation (EIONS) process. *Sep. Purif. Technol.* **215**, 190–207 (2019).
42. Farmer, J. C. et al. Electrosorption of chromium ions on carbon aerogel electrodes as a means of remediating ground water. *Energy Fuels* **11**, 337–347 (1997).
43. Saeed, A., Akhter, M. W. & Iqbal, M. Removal and recovery of heavy metals from aqueous solution using papaya wood as a new biosorbent. *Sep. Purif. Technol.* **45**, 25–31 (2005).
44. Hu, L., Mei, J.-y, Chen, Q.-w., Zhang, P. & Yan, N. Magnetically separable Prussian blue analogue $Mn_3[Co(CN)_6]_2 \cdot nH_2O$ porous nanocubes as excellent absorbents for heavy metal ions. *Nanoscale* **3**, 4270–4274 (2011).
45. Su, X. et al. Electrochemically-mediated selective capture of heavy metal chromium and arsenic oxyanions from water. *Nat. Commun.* **9**, 4701 (2018).
46. Farmer, J. C., Fix, D. V., Mack, G. V., Pekala, R. W. & Poco, J. F. Capacitive deionization of NH_4ClO_4 solutions with carbon aerogel electrodes. *J. Appl. Electrochem.* **26**, 1007–1018 (1996).
47. Farmer, J. C., Fix, D. V., Mack, G. V., Pekala, R. W. & Poco, J. F. Capacitive deionization of NaCl and $NaNO_3$ solutions with carbon aerogel electrodes. *J. Electrochem. Soc.* **143**, 159–169 (1996).
48. Lee, J., Yu, S.-H., Kim, C., Sung, Y.-E. & Yoon, J. Highly selective lithium recovery from brine using a λ-MnO_2–Ag battery. *Phys. Chem. Chem. Phys.* **15**, 7690–7695 (2013).
49. Siekierka, A., Tomaszewska, B. & Bryjak, M. Lithium capturing from geothermal water by hybrid capacitive deionization. *Desalination* **436**, 8–14 (2018).
50. Pasta, M., Battistel, A. & La Mantia, F. Batteries for lithium recovery from brines. *Energy Environ. Sci.* **5**, 9487–9491 (2012).
This study reported that desalination batteries can selectively extract lithium.
51. Trócoli, R., Battistel, A. & La Mantia, F. Nickel hexacyanoferrate as suitable alternative to Ag for electrochemical lithium recovery. *ChemSusChem* **8**, 2514–2519 (2015).
52. Kim, S., Kim, J., Kim, S., Lee, J. & Yoon, J. Electrochemical lithium recovery and organic pollutant removal from industrial wastewater of a battery recycling plant. *Environ. Sci. Water Res. Technol.* **4**, 175–182 (2018).
53. Kim, S., Yoon, H., Shin, D., Lee, J. & Yoon, J. Electrochemical selective ion separation in capacitive deionization with sodium manganese oxide. *J. Colloid Interface Sci.* **506**, 644–648 (2017).
54. Yoon, H., Lee, J., Kim, S. & Yoon, J. Electrochemical sodium ion impurity removal system for producing high purity KCl. *Hydrometallurgy* **175**, 354–358 (2018).
55. Yoon, H. et al. Capacitive deionization with Ca-alginate coated-carbon electrode for hardness control. *Desalination* **392**, 46–53 (2016).
56. Dykstra, J. E., Dijkstra, J., van der Wal, A., Hamelers, H. V. M. & Porada, S. On-line method to study dynamics of ion adsorption from mixtures of salts in capacitive deionization. *Desalination* **390**, 47–52 (2016).
57. Srimuk, P. et al. Potential-dependent, switchable ion selectivity in aqueous media using titanium disulfide. *ChemSusChem* **11**, 2091–2100 (2018).
58. Wang, Y. L. et al. High-performance capacitive deionization disinfection of water with graphene oxide-*graft*-quaternized chitosan nanohybrid electrode coating. *ACS Nano* **9**, 10142–10157 (2015).
59. Kim, T., Yu, J., Kim, C. & Yoon, J. Hydrogen peroxide generation in flow-mode capacitive deionization. *J. Electroanal. Chem.* **776**, 101–104 (2016).
60. Kim, S. et al. Hybrid electrochemical desalination system combined with an oxidation process. *ACS Sustain. Chem. Eng.* **6**, 1620–1626 (2018).
61. Bijmans, M. F. M. et al. CAPMIX-deploying capacitors for salt gradient power extraction. *Energy Procedia* **20**, 108–115 (2012).
62. Janssen, M., Härtel, A. & van Roij, R. Boosting capacitive blue-energy and desalination devices with waste heat. *Phys. Rev. Lett.* **113**, 268501 (2014).
63. Härtel, A., Janssen, M., Weingarth, D., Presser, V. & van Roij, R. Heat-to-current conversion of low-grade heat from a thermocapacitive cycle by supercapacitors. *Energy Environ. Sci.* **8**, 2396–2401 (2015).
64. Sales, B. B. et al. Direct power production from a water salinity difference in a membrane-modified supercapacitor flow cell. *Environ. Sci. Technol.* **44**, 5661–5665 (2010).
65. Sales, B. B. et al. Extraction of energy from small thermal differences near room temperature using capacitive membrane technology. *Environ. Sci. Technol. Lett.* **1**, 356–360 (2014).
66. Shapira, B., Cohen, I., Penki, T. R., Avraham, E. & Aurbach, D. Energy extraction and water treatment in one system: The idea of using a desalination battery in a cooling tower. *J. Power Sources* **378**, 146–152 (2018).
67. Soffer, A. & Folman, M. The electrical double layer of high surface porous carbon electrode. *J. Electroanal. Chem. Interf. Electrochem.* **38**, 25–43 (1972).
68. Biesheuvel, P. M. et al. Capacitive Deionization — defining a class of desalination technologies. Preprint at *arXiv* https://arxiv.org/abs/1709.05925 (2017).
69. Laheäär, A., Przygocki, P., Abbas, Q. & Béguin, F. Appropriate methods for evaluating the efficiency and capacitive behavior of different types of supercapacitors. *Electrochem. Commun.* **60**, 21–25 (2015).
70. Brousse, T., Bélanger, D. & Long, J. W. To be or not to be pseudocapacitive? *J. Electrochem. Soc.* **162**, A5185–A5189 (2015).
71. Suss, M. E. et al. Water desalination via capacitive deionization: what is it and what can we expect from it? *Energy Environ. Sci.* **8**, 2296–2319 (2015).
A review article on CDI.
72. Zhao, R. et al. Time-dependent ion selectivity in capacitive charging of porous electrodes. *J. Colloid Interface Sci.* **384**, 38–44 (2012).
73. Su, X., Kulik, H. J., Jamison, T. F. & Hatton, T. A. Anion-selective redox electrodes: electrochemically mediated separation with heterogeneous organometallic interfaces. *Adv. Funct. Mater.* **26**, 3394–3404 (2016).
74. Byles, B. W., Hayes-Oberst, B. & Pomerantseva, E. Ion removal performance, structural/compositional dynamics, and electrochemical stability of layered manganese oxide electrodes in hybrid capacitive deionization. *ACS Appl. Mater. Interfaces* **10**, 32313–32322 (2018).
75. Bao, W. et al. Porous cryo-dried MXene for efficient capacitive deionization. *Joule* **2**, 778–787 (2018).
76. Lee, J. et al. Pseudocapacitive desalination of brackish water and seawater with vanadium-pentoxide-decorated multiwalled carbon nanotubes. *ChemSusChem* **10**, 3611–3623 (2017).
77. Avraham, E., Bouhadana, Y., Soffer, A. & Aurbach, D. Limitation of charge efficiency in capacitive deionization. I. On the behavior of single activated carbon. *J. Electrochem. Soc.* **156**, P95–P99 (2009).
78. Avraham, E., Noked, M., Bouhadana, Y., Soffer, A. & Aurbach, D. Limitations of charge efficiency in capacitive deionization. II. On the behavior of CDI cells comprising two activated carbon electrodes. *J. Electrochem. Soc.* **156**, P157–P162 (2009).
79. Prehal, C. et al. Tracking the structural arrangement of ions in carbon supercapacitor nanopores using in situ small-angle X-ray scattering. *Energy Environ. Sci.* **8**, 1725–1735 (2015).
80. Shapira, B., Avraham, E. & Aurbach, D. Side reactions in capacitive deionization (CDI) processes: the role of oxygen reduction. *Electrochim. Acta* **220**, 285–295 (2016).
81. Suss, M. E. et al. Capacitive desalination with flow-through electrodes. *Energy Environ. Sci.* **5**, 9511–9519 (2012).
82. Kim, T. & Yoon, J. CDI ragone plot as a functional tool to evaluate desalination performance in capacitive deionization. *RSC Adv.* **5**, 1456–1461 (2015).
83. Christen, T. & Carlen, M. W. Theory of Ragone plots. *J. Power Sources* **91**, 210–216 (2000).
84. Ragone, D. V. in *Society of Automotive Engineers Mid-Year Meeting 1968* 1–12 (Society of Automotive Engineers, 1968).
85. Zhang, X., Zuo, K., Zhang, X., Zhang, C. & Liang, P. Selective ion separation by capacitive deionization (CDI) based technologies: a state-of-the-art review. *Environ. Sci. Water Res. Technol.* **6**, 243–257 (2020).
Review article on the selective separation by CDI.
86. Oyarzun, D. I., Hemmatifar, A., Palko, J. W., Stadermann, M. & Santiago, J. G. Adsorption and capacitive regeneration of nitrate using inverted capacitive deionization with surfactant functionalized carbon electrodes. *Sep. Purif. Technol.* **194**, 410–415 (2018).
87. Su, X. & Hatton, T. A. Redox-electrodes for selective electrochemical separations. *Adv. Colloid Interface Sci.* **244**, 6–20 (2017).
88. Seader, J. D., Henley, E. J. & Roper, D. K. in *Separation Process Principles: Chemical and Biochemical Operations* 3rd edn Vol. 18 (Wiley, 2010).
89. Sun, B. et al. Separation of low concentration of cesium ion from wastewater by electrochemically switched ion exchange method: experimental adsorption kinetics analysis. *J. Hazard. Mater.* **233–234**, 177–183 (2012).
90. Wang, L., Dykstra, J. E. & Lin, S. Energy efficiency of capacitive deionization. *Environ. Sci. Technol.* **53**, 3366–3378 (2019).
91. Hemmatifar, A., Palko, J. W., Stadermann, M. & Santiago, J. G. Energy breakdown in capacitive deionization. *Water Res.* **104**, 303–311 (2016).
92. Hawks, S. A. et al. Performance metrics for the objective assessment of capacitive deionization systems. *Water Res.* **152**, 126–137 (2019).
93. Tan, C., He, C., Fletcher, J. & Waite, T. D. Energy recovery in pilot scale membrane CDI treatment of brackish waters. *Water Res.* **168**, 115146 (2020).
94. Qu, Y. et al. Energy consumption analysis of constant voltage and constant current operations in capacitive deionization. *Desalination* **400**, 18–24 (2016).
95. Gogotsi, Y. & Simon, P. True performance metrics in electrochemical energy storage. *Science* **334**, 917–918 (2011).
96. Długołęcki, P. & van der Wal, A. Energy recovery in membrane capacitive deionization. *Environ. Sci. Technol.* **47**, 4904–4910 (2013).
97. Hand, S., Shang, X., Guest, J. S., Smith, K. C. & Cusick, R. D. Global sensitivity analysis to characterize operational limits and prioritize performance goals of

capacitive deionization technologies. *Environ. Sci. Technol.* **53**, 3748–3756 (2019).
98. Hand, S., Guest, J. S. & Cusick, R. D. Technoeconomic analysis of brackish water capacitive deionization: navigating tradeoffs between performance, lifetime, and material costs. *Environ. Sci. Technol.* **53**, 13353–13363 (2019).
99. Landon, J., Gao, X., Omosebi, A. & Liu, K. Progress and outlook for capacitive deionization technology. *Curr. Opin. Chem. Eng.* **25**, 1–8 (2019).
100. Moreno, D. & Hatzell, M. C. Efficiency of carnot and conventional capacitive deionization cycles. *J. Phys. Chem. C* **122**, 22480–22486 (2018).
101. Smith, K. C. Theoretical evaluation of electrochemical cell architectures using cation intercalation electrodes for desalination. *Electrochim. Acta* **230**, 333–341 (2017).
This study introduced the sodium-ion-desalination concept.
102. Arulrajan, A. C. et al. Exceptional water desalination performance with anion-selective electrodes. *Adv. Mater.* **31**, 1806937 (2019).
103. Nam, D.-H. & Choi, K.-S. Electrochemical desalination using Bi/BiOCl electrodialysis cells. *ACS Sustain. Chem. Eng.* **6**, 15455–15462 (2018).
104. Kim, N. et al. Short review of multichannel membrane capacitive deionization: principle, current status, and future prospect. *Appl. Sci.* **10**, 683 (2020).
Review article on multichannel membrane CDI.
105. Kim, C., Srimuk, P., Lee, J. & Presser, V. Enhanced desalination via cell voltage extension of membrane capacitive deionization using an aqueous/organic bi-electrolyte. *Desalination* **443**, 56–61 (2018).
106. Doornbusch, G. J., Dykstra, J. E., Biesheuvel, P. M. & Suss, M. E. Fluidized bed electrodes with high carbon loading for water desalination by capacitive deionization. *J. Mater. Chem. A* **4**, 3642–3647 (2016).
107. Rommerskirchen, A., Gendel, Y. & Wessling, M. Single module flow-electrode capacitive deionization for continuous water desalination. *Electrochem. Commun.* **60**, 34–37 (2015).
108. Beh, E. S., Benedict, M. A., Desai, D. & Rivest, J. B. A redox-shuttled electrochemical method for energy-efficient separation of salt from water. *ACS Sustain. Chem. Eng.* **7**, 13411–13417 (2019).
109. Liang, Q. et al. An organic flow desalination battery. *Energy Storage Mater.* **20**, 203–207 (2019).
110. Tang, W., He, D., Zhang, C., Kovalsky, P. & Waite, T. D. Comparison of Faradaic reactions in capacitive deionization (CDI) and membrane capacitive deionization (MCDI) water treatment processes. *Water Res.* **120**, 229–237 (2017).
111. Le Fevre, L. W. et al. Cell optimisation of supercapacitors using a quasi-reference electrode and potentiostatic analysis. *J. Power Sources* **424**, 52–60 (2019).
112. Zornitta, R. L. et al. Charge and potential balancing for optimized capacitive deionization using lignin-derived, low-cost activated carbon electrodes. *ChemSusChem* **11**, 2101–2113 (2018).
113. Liu, Y. et al. Review on carbon-based composite materials for capacitive deionization. *RSC Adv.* **5**, 15205–15225 (2015).
114. Porada, S., Bryjak, M., van der Wal, A. & Biesheuvel, P. M. Effect of electrode thickness variation on operation of capacitive deionization. *Electrochim. Acta* **75**, 148–156 (2012).
115. Porada, S. et al. Water desalination using capacitive deionization with microporous carbon electrodes. *ACS Appl. Mater. Interfaces* **4**, 1194–1199 (2012).
116. Li, H. B., Zou, L. D., Pan, L. K. & Sun, Z. Novel graphene-like electrodes for capacitive deionization. *Environ. Sci. Technol.* **44**, 8692–8697 (2010).
117. Yan, C., Zou, L. & Short, R. Single-walled carbon nanotubes and polyaniline composites for capacitive deionization. *Desalination* **290**, 125–129 (2012).
118. Chang, L., Li, J., Duan, X. & Liu, W. Porous carbon derived from Metal–organic framework (MOF) for capacitive deionization electrode. *Electrochim. Acta* **176**, 956–964 (2015).
119. Schipper, F. et al. Study of cathode materials for lithium-ion batteries: recent progress and new challenges. *Inorganics* **5**, 32 (2017).
120. Wang, Z. et al. Nanoarchitectured metal–organic framework/polypyrrole hybrids for brackish water desalination using capacitive deionization. *Mater. Horiz.* **6**, 1433–1437 (2019).
121. Kim, T. et al. Enhanced charge efficiency and reduced energy use in capacitive deionization by increasing the discharge voltage. *J. Colloid Interface Sci.* **446**, 317–326 (2015).
122. Gao, X. et al. Complementary surface charge for enhanced capacitive deionization. *Water Res.* **92**, 275–282 (2016).
123. Gao, X., Omosebi, A., Landon, J. & Liu, K. L. Surface charge enhanced carbon electrodes for stable and efficient capacitive deionization using inverted adsorption–desorption behavior. *Energy Environ. Sci.* **8**, 897–909 (2015).
124. Porada, S., Feng, G., Suss, M. E. & Presser, V. Capacitive deionization in organic solutions: case study using propylene carbonate. *RSC Adv.* **6**, 5865–5870 (2016).
125. Kalluri, R. K. et al. Unraveling the potential and pore-size dependent capacitance of slit-shaped graphitic carbon pores in aqueous electrolytes. *Phys. Chem. Chem. Phys.* **15**, 2309–2320 (2013).
126. Bi, S. et al. Permselective ion electrosorption of subnanometer pores at high molar strength enables capacitive deionization of saline water. *Sustain. Energy Fuels* **4**, 1285–1295 (2020).
127. Tang, W. et al. Various cell architectures of capacitive deionization: recent advances and future trends. *Water Res.* **150**, 225–251 (2019).
128. Kim, C., Lee, J., Srimuk, P., Aslan, M. & Presser, V. Concentration-gradient multichannel flow-stream membrane capacitive deionization cell for high desalination capacity of carbon electrodes. *ChemSusChem* **10**, 4914–4920 (2017).
129. Kim, C., Srimuk, P., Lee, J., Aslan, M. & Presser, V. Semi-continuous capacitive deionization using multi-channel flow stream and ion exchange membranes. *Desalination* **425**, 104–110 (2018).
130. Kang, J. S. et al. Rapid inversion of surface charges in heteroatom-doped porous carbon: a route to robust electrochemical desalination. *Adv. Funct. Mater.* **30**, 1909387 (2019).
131. Xu, X. et al. Facile synthesis of novel graphene sponge for high performance capacitive deionization. *Sci. Rep.* **5**, 8458 (2015).
132. Xu, X., Sun, Z., Chua, D. H. C. & Pan, L. Novel nitrogen doped graphene sponge with ultrahigh capacitive deionization performance. *Sci. Rep.* **5**, 11225 (2015).
133. Gerischer, H., McIntyre, R., Scherson, D. & Storck, W. Density of the electronic states of graphite: derivation from differential capacitance measurements. *J. Phys. Chem.* **91**, 1930–1935 (1987).
134. Kornyshev, A. A., Luque, N. B. & Schmickler, W. Differential capacitance of ionic liquid interface with graphite: the story of two double layers. *J. Solid. State Electrochem.* **18**, 1345–1349 (2014).
135. Weingarth, D. et al. Graphitization as a universal tool to tailor the potential-dependent capacitance of carbon supercapacitors. *Adv. Energy Mater.* **4**, 1400316 (2014).
136. Paraknowitsch, J. P. & Thomas, A. Doping carbons beyond nitrogen: an overview of advanced heteroatom doped carbons with boron, sulphur and phosphorus for energy applications. *Energy Environ. Sci.* **6**, 2839–2855 (2013).
137. Xu, X., Pan, L., Liu, Y., Lu, T. & Sun, Z. Enhanced capacitive deionization performance of graphene by nitrogen doping. *J. Colloid Interface Sci.* **445**, 143–150 (2015).
138. Xu, X. et al. Capacitive deionization using nitrogen-doped mesostructured carbons for highly efficient brackish water desalination. *Chem. Eng. J.* **362**, 887–896 (2019).
139. He, D., Wong, C. E., Tang, W., Kovalsky, P. & Waite, T. D. Faradaic reactions in water desalination by batch-mode capacitive deionization. *Environ. Sci. Technol. Lett.* **3**, 222–226 (2016).
140. Srimuk, P. et al. High performance stability of titania decorated carbon for desalination with capacitive deionization in oxygenated water. *RSC Adv.* **6**, 106081–106089 (2016).
141. Singh, K., Porada, S., de Gier, H. D., Biesheuvel, P. M. & de Smet, L. C. P. M. Timeline on the application of intercalation materials in capacitive deionization. *Desalination* **455**, 115–134 (2019).
142. Privett, B. J., Shin, J. H. & Schoenfisch, M. H. Electrochemical sensors. *Anal. Chem.* **82**, 4723–4741 (2010).
143. Muench, S. et al. Polymer-based organic batteries. *Chem. Rev.* **116**, 9438–9484 (2016).
144. Zhang, B. et al. Redox gated polymer memristive processing memory unit. *Nat. Commun.* **10**, 736 (2019).
145. Beer, P. D. & Gale, P. A. Anion recognition and sensing: the state of the art and future perspectives. *Angew. Chem. Int. Ed.* **40**, 486–516 (2001).
146. Achilleos, D. S. & Hatton, T. A. Selective molecularly mediated pseudocapacitive separation of ionic species in solution. *ACS Appl. Mater. Interfaces* **8**, 32743–32753 (2016).
147. Kim, K. et al. Asymmetric redox-polymer interfaces for electrochemical reactive separations: synergistic capture and conversion of arsenic. *Adv. Mater.* **32**, 1906877 (2020).
148. Raudsepp, T., Marandi, M., Tamm, T., Sammelselg, V. & Tamm, J. Influence of ion-exchange on the electrochemical properties of polypyrrole films. *Electrochim. Acta* **122**, 79–86 (2014).
149. Cui, H. et al. Defluoridation of water via electrically controlled anion exchange by polyaniline modified electrode reactor. *Water Res.* **45**, 5736–5744 (2011).
150. Kim, Y., Lin, Z., Jeon, I., Van Voorhis, T. & Swager, T. M. Polyaniline nanofiber electrodes for reversible capture and release of mercury(II) from water. *J. Am. Chem. Soc.* **140**, 14413–14420 (2018).
151. Ren, Y., Mao, X. & Hatton, T. A. An asymmetric electrochemical system with complementary tunability in hydrophobicity for selective separations of organics. *ACS Cent. Sci.* **5**, 1396–1406 (2019).
152. Kong, H., Yang, M., Miao, Y. C. & Zhao, X. Y. Polypyrrole as a novel chloride-storage electrode for seawater desalination. *Energy Technol.* **7**, 1900835 (2019).
153. Ahualli, S., Iglesias, G. R., Fernandez, M. M., Jimenez, M. L. & Delgado, A. V. Use of soft electrodes in capacitive deionization of solutions. *Environ. Sci. Technol.* **51**, 5326–5333 (2017).
154. Su, X. & Hatton, T. A. Electrosorption at functional interfaces: from molecular-level interactions to electrochemical cell design. *Phys. Chem. Chem. Phys.* **19**, 23570–23584 (2017).
155. Li, Y. et al. Novel hybrid capacitive deionization constructed by a redox-active covalent organic framework and its derived porous carbon for highly efficient desalination. *J. Mater. Chem. A* **7**, 25305–25313 (2019).
156. Chandra, S. et al. Chemically stable multilayered covalent organic nanosheets from covalent organic frameworks via mechanical delamination. *J. Am. Chem. Soc.* **135**, 17853–17861 (2013).
157. Huggins, R. A. *Advanced Batteries. Materials Science Aspects* Ch. 1.3 (Springer, 2009).
158. Augustyn, V. & Gogotsi, Y. 2D materials with nanoconfined fluids for electrochemical energy storage. *Joule* **1**, 443–452 (2017).
159. Guo, L. et al. A high performance electrochemical deionization method to desalinate brackish water with $FePO_4$/RGO nanocomposite. *J. Mater. Chem. A* **6**, 8901–8908 (2018).
160. Meng, J. et al. Advances in structure and property optimizations of battery electrode materials. *Joule* **1**, 522–547 (2017).
161. Kim, S., Lee, J., Kim, C. & Yoon, J. $Na_2FeP_2O_7$ as a novel material for hybrid capacitive deionization. *Electrochim. Acta* **203**, 265–271 (2016).
162. Srimuk, P. et al. Titanium disulfide: a promising low-dimensional electrode material for sodium ion intercalation for sea water desalination. *Chem. Mater.* **29**, 9964–9973 (2017).
163. Kim, H. et al. Ab initio study of the sodium intercalation and intermediate phases in $Na_{0.44}MnO_2$ for sodium-ion battery. *Chem. Mater.* **24**, 1205–1211 (2012).
164. Sauvage, F., Laffont, L., Tarascon, J. M. & Baudrin, E. Study of the insertion/deinsertion mechanism of sodium into $Na_{0.44}MnO_2$. *Inorg. Chem.* **46**, 3289–3294 (2007).
165. Moreau, P., Guyomard, D., Gaubicher, J. & Boucher, F. Structure and stability of sodium intercalated phases in olivine $FePO_4$. *Chem. Mater.* **22**, 4126–4128 (2010).
166. Dai, D. et al. Analysis of the spin exchange interactions and the ordered magnetic structures of lithium transition metal phosphates $LiMPO_4$ (M=Mn, Fe, Co, Ni) with the olivine structure. *Inorg. Chem.* **44**, 2407–2413 (2005).
167. Tan, C. et al. Recent advances in ultrathin two-dimensional nanomaterials. *Chem. Rev.* **117**, 6225–6331 (2017).
168. Wang, B. et al. Prussian blue analogs for rechargeable batteries. *iScience* **3**, 110–133 (2018).
169. Mathis, T. S. et al. Energy storage data reporting in perspective — guidelines for interpreting the performance of electrochemical energy storage systems. *Adv. Energy Mater.* **9**, 1902007 (2019).
170. Srimuk, P. et al. In situ tracking of partial sodium desolvation of materials with capacitive, pseudocapacitive, and battery-like charge/discharge behavior in aqueous electrolytes. *Langmuir* **34**, 13132–13143 (2018).

171. Ridley, P., Andris, R. & Pomerantseva, E. HCDI performance of Na-2x3 and Na-2x4 nanowires for water desalination. *SPIE Proc.* **11085**, 110851J (2019).
172. Byles, B. W., Cullen, D. A., More, K. L. & Pomerantseva, E. Tunnel structured manganese oxide nanowires as redox active electrodes for hybrid capacitive deionization. *Nano Energy* **44**, 476–488 (2018).
173. Leong, Z. Y. & Yang, H. Y. A study of MnO_2 with different crystalline forms for pseudocapacitive desalination. *ACS Appl. Mater. Interfaces* **11**, 13176–13184 (2019).
174. Nayak, P. K., Yang, L., Brehm, W. & Adelhelm, P. From lithium-ion to sodium-ion batteries: advantages, challenges, and surprises. *Angew. Chem. Int. Ed.* **57**, 102–120 (2018).
175. Naguib, M. et al. Two-dimensional transition metal carbides. *ACS Nano* **6**, 1322–1331 (2012).
176. Anasori, B., Lukatskaya, M. R. & Gogotsi, Y. 2D metal carbides and nitrides (MXenes) for energy storage. *Nat. Rev. Mater.* **2**, 16098 (2017).
177. Augustyn, V., Simon, P. & Dunn, B. Pseudocapacitive oxide materials for high-rate electrochemical energy storage. *Energy Environ. Sci.* **7**, 1597–1614 (2014).
178. Lee, J. et al. Sodium ion removal by hydrated vanadyl phosphate for electrochemical water desalination. *J. Mater. Chem. A* **7**, 4175–4184 (2019).
179. Levi, M. D. et al. Solving the capacitive paradox of 2D MXene using electrochemical quartz-crystal admittance and in situ electronic conductance measurements. *Adv. Energy Mater.* **5**, 1400815 (2015).
180. Shpigel, N. et al. Direct assessment of nanoconfined water in 2D Ti_3C_2 electrode interspaces by a surface acoustic technique. *J. Am. Chem. Soc.* **140**, 8910–8917 (2018).
181. Naguib, M. et al. Two-dimensional nanocrystals produced by exfoliation of Ti_3AlC_2. *Adv. Mater.* **23**, 4248–4253 (2011).
182. Qian, A., Seo, J. Y., Shi, H., Lee, J. Y. & Chung, C.-H. Surface functional groups and electrochemical behavior in dimethyl sulfoxide-delaminated $Ti_3C_2T_x$ MXene. *ChemSusChem* **11**, 3719–3723 (2018).
183. Schultz, T. et al. Surface termination dependent work function and electronic properties of $Ti_3C_2T_x$ MXene. *Chem. Mater.* **31**, 6590–6597 (2019).
184. Srimuk, P. et al. Two-dimensional molybdenum carbide (MXene) with divacancy ordering for brackish and sea water desalination via cation and anion intercalation. *ACS Sustain. Chem. Eng.* **6**, 3739–3747 (2018).
185. Huang, S. & Mochalin, V. N. Hydrolysis of 2D transition-metal carbides (MXenes) in colloidal solutions. *Inorg. Chem.* **58**, 1958–1966 (2019).
186. Coleman, J. N. et al. Two-dimensional nanosheets produced by liquid exfoliation of layered Materials. *Science* **331**, 568–571 (2011).
187. Huang, W., Luo, X., Gan, C. K., Quek, S. Y. & Liang, G. Theoretical study of thermoelectric properties of few-layer MoS_2 and WSe_2. *Phys. Chem. Chem. Phys.* **16**, 10866–10874 (2014).
188. Srimuk, P. et al. Faradaic deionization of brackish and sea water via pseudocapacitive cation and anion intercalation into few layered molybdenum disulfide. *J. Mater. Chem. A* **5**, 15640–15649 (2017).
189. Wang, Q. H., Kalantar-Zadeh, K., Kis, A., Coleman, J. N. & Strano, M. S. Electronics and optoelectronics of two-dimensional transition metal dichalcogenides. *Nat. Nanotechnol.* **7**, 699–712 (2012).
190. He, H. et al. Structural properties and phase transition of Na adsorption on monolayer MoS_2. *Nanoscale Res. Lett.* **11**, 330 (2016).
191. Wang, X. et al. In situ electron microscopy investigation of sodiation of titanium disulfide nanoflakes. *ACS Nano* **13**, 9421–9430 (2019).
192. Mitchell, J. B., Lo, W. C., Genc, A., LeBeau, J. & Augustyn, V. Transition from battery to pseudocapacitor behavior via structural water in tungsten oxide. *Chem. Mater.* **29**, 3928–3937 (2017).
193. Feng, Q., Kanoh, H. & Ooi, K. Manganese oxide porous crystals. *J. Mater. Chem.* **9**, 319–333 (1999).
194. Pinna, N., Willinger, M., Weiss, K., Urban, J. & Schlögl, R. Local structure of nanoscopic materials: V_2O_5 nanorods and nanowires. *Nano Lett.* **3**, 1131–1134 (2003).
195. Moretti, A. & Passerini, S. Bilayered nanostructured $V_2O_5 \cdot nH_2O$ for metal batteries. *Adv. Energy Mater.* **6**, 1600868 (2016).
196. Masquelier, C. & Croguennec, L. Polyanionic (phosphates, silicates, sulfates) frameworks as electrode materials for rechargeable Li (or Na) batteries. *Chem. Rev.* **113**, 6552–6591 (2013).
197. Zhu, Y., Peng, L., Chen, D. & Yu, G. Intercalation pseudocapacitance in ultrathin $VOPO_4$ nanosheets: toward high-rate alkali-ion-based electrochemical energy storage. *Nano Lett.* **16**, 742–747 (2016).
198. Paulitsch, B., Yun, J. & Bandarenka, A. S. Electrodeposited $Na_2VO_x[Fe(CN)_6]$ films as a cathode material for aqueous Na-ion batteries. *ACS Appl. Mater. Interfaces* **9**, 8107–8112 (2017).
199. Lee, J. et al. Enhancement in desalination performance of battery electrodes via improved mass transport using a multichannel flow system. *ACS Appl. Mater. Interfaces* **11**, 36580–36588 (2019).
200. Ding, J., Hu, W., Paek, E. & Mitlin, D. Review of hybrid ion capacitors: from aqueous to lithium to sodium. *Chem. Rev.* **118**, 6457–6498 (2018).
201. Zhao, W., Guo, L., Ding, M., Huang, Y. & Yang, H. Y. Ultrahigh-desalination-capacity dual-ion electrochemical deionization device based on $Na_3V_2(PO_4)_3$@C–AgCl electrodes. *ACS Appl. Mater. Interfaces* **10**, 40540–40548 (2018).
202. Wang, Z., Gong, H., Zhang, Y., Liang, P. & Wang, K. Nitrogen recovery from low-strength wastewater by combined membrane capacitive deionization (MCDI) and ion exchange (IE) process. *Chem. Eng. J.* **316**, 1–6 (2017).
203. Mossad, M. & Zou, L. Study of fouling and scaling in capacitive deionisation by using dissolved organic and inorganic salts. *J. Hazard. Mater.* **244–245**, 387–393 (2013).
204. Zhang, W., Mossad, M. & Zou, L. A study of the long-term operation of capacitive deionisation in inland brackish water desalination. *Desalination* **320**, 80–85 (2013).
205. Liu, X., Whitacre, J. F. & Mauter, M. S. Mechanisms of humic acid fouling on capacitive and insertion electrodes for electrochemical desalination. *Environ. Sci. Technol.* **52**, 12633–12641 (2018).
206. Stone, A. T. & Morgan, J. J. Reduction and dissolution of manganese(III) and manganese(IV) oxides by organics: 2. Survey of the reactivity of organics. *Environ. Sci. Technol.* **18**, 617–624 (1984).
207. Bates, R. G. & Macaskill, J. B. Standard potential of the silver-silver chloride electrode. *Pure Appl. Chem.* **50**, 1701–1706 (1978).
208. Cai, P. F. et al. Capacitive deionization of seawater effected by nano Ag and Ag@C on graphene. *Mar. Pollut. Bull.* **85**, 733–737 (2014).
209. Chen, F., Huang, Y., Guo, L., Ding, M. & Yang, H. Y. A dual-ion electrochemistry deionization system based on AgCl-$Na_{0.44}MnO_2$ electrodes. *Nanoscale* **9**, 10101–10108 (2017).
210. Yoon, H., Lee, J., Kim, S. & Yoon, J. Hybrid capacitive deionization with Ag coated carbon composite electrode. *Desalination* **422**, 42–48 (2017).
211. Huang, Y. et al. Low energy consumption dual-ion electrochemical deionization system using $NaTi_2(PO_4)_3$-AgNPs electrodes. *Desalination* **451**, 241–247 (2019).
212. Zhao, W., Ding, M., Guo, L. & Yang, H. Y. Dual-ion electrochemical deionization system with binder-free aerogel electrodes. *Small* **15**, 1805505 (2019).
213. Fighera, M., van der Wal, P. D. & Shea, H. Microfluidic platform for seawater desalination by coulometric removal of chloride ions through printed Ag electrodes. *J. Electrochem. Soc.* **164**, H836–H845 (2017).
214. Lee, J. et al. Redox-electrolytes for non-flow electrochemical energy storage: a critical review and best practice. *Prog. Mater. Sci.* **101**, 46–89 (2019).
215. Bandaru, P. R., Yamada, H., Narayanan, R. & Hoefer, M. Charge transfer and storage in nanostructures. *Mater. Sci. Eng. R Rep.* **96**, 1–69 (2015).
216. Narayanan, R. & Bandaru, P. R. High rate capacity through redox electrolytes confined in macroporous electrodes. *J. Electrochem. Soc.* **162**, A86–A91 (2015).
217. Desai, D. et al. Electrochemical desalination of seawater and hypersaline brines with coupled electricity storage. *ACS Energy Lett.* **3**, 375–379 (2018).
218. Hou, X. et al. Coupling desalination and energy storage with redox flow electrodes. *Nanoscale* **10**, 12308–12314 (2018).
219. Kim, N., Hong, S. P., Lee, J., Kim, C. & Yoon, J. High desalination performance via redox couple reaction in the multi-channel capacitive deionization system. *ACS Sustain. Chem. Eng.* **7**, 16182–16189 (2019).
220. Chen, L., Bai, H., Huang, Z. & Li, L. Mechanism investigation and suppression of self-discharge in active electrolyte enhanced supercapacitors. *Energy Environ. Sci.* **7**, 1750–1759 (2014).
221. Lee, J. et al. Tin/vanadium redox electrolyte for battery-like energy storage capacity combined with supercapacitor-like power handling. *Energy Environ. Sci.* **9**, 3392–3398 (2016).
222. Cohen, I., Shapira, B., Avraham, E., Soffer, A. & Aurbach, D. Bromide ions specific removal and recovery by electrochemical desalination. *Environ. Sci. Technol.* **52**, 6275–6281 (2018).
223. Kickelbick, G. *Hybrid Materials: Synthesis, Characterization, and Applications* (Wiley-VCH, 2007).
224. Fleischmann, S., Tolosa, A. & Presser, V. Design of carbon/metal oxide hybrids for electrochemical energy storage. *Chem. Eur. J.* **24**, 12143–12153 (2018).
225. Levi, M. D. et al. In situ tracking of ion insertion in iron phosphate olivine electrodes via electrochemical quartz crystal admittance. *J. Phys. Chem. C* **117**, 1247–1256 (2013).
226. Kumar, A., Fukuda, H., Hatton, T. A. & Lienhard, J. H. Lithium recovery from oil and gas produced water: a need for a growing energy industry. *ACS Energy Lett.* **4**, 1471–1474 (2019).
227. Turcheniuk, K., Bondarev, D., Singhal, V. & Yushin, G. Ten years left to redesign lithium-ion batteries. *Nature* **559**, 467–470 (2018).
228. Epstein, J. A., Feist, E. M., Zmora, J. & Marcus, Y. Extraction of lithium from the dead sea. *Hydrometallurgy* **6**, 269–275 (1981).
229. Kavanagh, L., Keohane, J., Cabellos, G. G., Lloyd, A. & Cleary, J. Global lithium sources - industrial use and future in the electric vehicle industry: a review. *Resources* **7**, 57 (2018).
230. Bryjak, M., Siekierka, A., Kujawski, J., Smolińska-Kempisty, K. & Kujawski, W. Capacitive deionization for selective extraction of lithium from aqueous solutions. *J. Membr. Sep. Technol.* **4**, 110–115 (2015).
231. Calvo, E. J. Electrochemical methods for sustainable recovery of lithium from natural brines and battery recycling. *Curr. Opin. Electrochem.* **15**, 102–108 (2019).
232. Yu, J., Wang, X., Zhou, M. & Wang, Q. A redox targeting-based material recycling strategy for spent lithium ion batteries. *Energy Environ. Sci.* **12**, 2672–2677 (2019).
233. Bain, E. J., Calo, J. M., Spitz-Steinberg, R., Kirchner, J. & Axén, J. Electrosorption/electrodesorption of arsenic on a granular activated carbon in the presence of other heavy metals. *Energy Fuels* **24**, 3415–3421 (2010).
234. Liu, Y.-X., Yuan, D.-X., Yan, J.-M., Li, Q.-L. & Ouyang, T. Electrochemical removal of chromium from aqueous solutions using electrodes of stainless steel nets coated with single wall carbon nanotubes. *J. Hazard. Mater.* **186**, 473–480 (2011).
235. Choi, J., Dorji, P., Shon, H. K. & Hong, S. Applications of capacitive deionization: Desalination, softening, selective removal, and energy efficiency. *Desalination* **449**, 118–130 (2019).
236. Huang, Z., Lu, L., Cai, Z. & Ren, Z. J. Individual and competitive removal of heavy metals using capacitive deionization. *J. Hazard. Mater.* **302**, 323–331 (2016).
237. Fan, C. S., Liou, S. Y. H. & Hou, C. H. Capacitive deionization of arsenic-contaminated groundwater in a single-pass mode. *Chemosphere* **184**, 924–931 (2017).
238. Gaikwad, M. S. & Balomajumder, C. Simultaneous electrosorptive removal of chromium(VI) and fluoride ions by capacitive deionization (CDI): Multicomponent isotherm modeling and kinetic study. *Sep. Purif. Technol.* **186**, 272–281 (2017).
239. Zhang, M., Jia, F., Dai, M. & Song, S. Combined electrosorption and chemisorption of low concentration Pb(II) from aqueous solutions with molybdenum disulfide as electrode. *Appl. Surf. Sci.* **455**, 258–266 (2018).
240. Suss, M. E. Size-based ion selectivity of micropore electric double layers in capacitive deionization electrodes. *J. Electrochem. Soc.* **164**, E270–E275 (2017).
241. Guyes, E. N., Malka, T. & Suss, M. E. Enhancing the ion-size-based selectivity of capacitive deionization electrodes. *Environ. Sci. Technol.* **53**, 8447–8454 (2019).
242. Srimuk, P., Wang, L., Budak, Ö. & Presser, V. High-performance ion removal via zinc–air desalination. *Electrochem. Commun.* https://doi.org/10.1016/j.elecom.2020.106713 (2020).
243. Liu, X., Shanbhag, S. & Mauter, M. S. Understanding and mitigating performance decline in electrochemical deionization. *Curr. Opin. Chem. Eng.* **25**, 67–74 (2019).
244. Tsouris, C. et al. Mesoporous carbon for capacitive deionization of saline water. *Environ. Sci. Technol.* **45**, 10243–10249 (2011).

245. Kong, W. et al. Holey graphene hydrogel with in-plane pores for high-performance capacitive desalination. *Nano Res.* **9**, 2458–2466 (2016).
246. Dai, K., Shi, L., Fang, J., Zhang, D. & Yu, B. NaCl adsorption in multi-walled carbon nanotubes. *Mater. Lett.* **59**, 1989–1992 (2005).
247. Liu, N.-L. et al. ZIF-8 derived, nitrogen-doped porous electrodes of carbon polyhedron particles for high-performance electrosorption of salt ions. *Sci. Rep.* **6**, 28847 (2016).
248. Xu, X., Wang, M., Liu, Y., Lu, T. & Pan, L. Metal–organic framework-engaged formation of a hierarchical hybrid with carbon nanotube inserted porous carbon polyhedra for highly efficient capacitive deionization. *J. Mater. Chem. A* **4**, 5467–5473 (2016).
249. Zhang, J. et al. N, P, S co-doped hollow carbon polyhedra derived from MOF-based core-shell nanocomposites for capacitive deionization. *J. Mater. Chem. A* **6**, 15245–15252 (2018).
250. Liu, Y. et al. Metal–organic framework-derived porous carbon polyhedra for highly efficient capacitive deionization. *Chem. Commun.* **51**, 12020–12023 (2015).
251. Chang, L., Li, J., Duan, X. & Liu, W. Porous carbon derived from Metal–organic framework (MOF) for capacitive deionization electrode. *Electrochim. Acta* **176**, 956–964 (2015).
252. Chen, B. et al. Enhanced capacitive desalination of MnO_2 by forming composite with multi-walled carbon nanotubes. *RSC Adv.* **6**, 6730–6736 (2016).
253. Wu, T. et al. Highly stable hybrid capacitive deionization with a MnO_2 anode and a positively charged cathode. *Environ. Sci. Technol. Lett.* **5**, 98–102 (2018).
254. Porada, S., Shrivastava, A., Bukowska, P., Biesheuvel, P. M. & Smith, K. C. Nickel hexacyanoferrate electrodes for continuous cation intercalation desalination of brackish water. *Electrochim. Acta* **255**, 369–378 (2017).
255. Kim, T., Gorski, C. A. & Logan, B. E. Low energy desalination using battery electrode deionization. *Environ. Sci. Technol. Lett.* **4**, 444–449 (2017).
256. Guo, L. et al. A Prussian blue anode for high performance electrochemical deionization promoted by the faradaic mechanism. *Nanoscale* **9**, 13305–13312 (2017).
257. Choi, S. et al. Battery electrode materials with omnivalent cation storage for fast and charge-efficient ion removal of asymmetric capacitive deionization. *Adv. Funct. Mater.* **28**, 1802665 (2018).
258. Ding, Z. et al. Significantly improved stability of hybrid capacitive deionization using nickel hexacyanoferrate/reduced graphene oxide cathode at low voltage operation. *Desalination* **468**, 114078 (2019).
259. Vafakhah, S. et al. Efficient sodium-ion intercalation into the freestanding Prussian blue/graphene aerogel anode in a hybrid capacitive deionization system. *ACS Appl. Mater. Interfaces* **11**, 5989–5998 (2019).
260. Han, C., Meng, Q., Cao, B. & Tian, G. Enhanced hybrid capacitive deionization performance by sodium titanium phosphate/reduced porous graphene oxide composites. *ACS Omega* **4**, 11455–11463 (2019).
261. Cao, J., Wang, Y., Wang, L., Yu, F. & Ma, J. $Na_3V_2(PO_4)_3$@C as Faradaic electrodes in capacitive deionization for high-performance desalination. *Nano Lett.* **19**, 823–828 (2019).
262. Huang, Y., Chen, F., Guo, L. & Yang, H. Y. Ultrahigh performance of a novel electrochemical deionization system based on a $NaTi_2(PO_4)_3$/rGO nanocomposite. *J. Mater. Chem. A* **5**, 18157–18165 (2017).
263. Lukatskaya, M. R., Dunn, B. & Gogotsi, Y. Multidimensional materials and device architectures for future hybrid energy storage. *Nat. Commun.* **7**, 12647 (2016).
264. Kim, C. et al. Influence of pore structure and cell voltage of activated carbon cloth as a versatile electrode material for capacitive deionization. *Carbon* **122**, 329–335 (2017).
265. Chun, S.-E. et al. Design of aqueous redox-enhanced electrochemical capacitors with high specific energies and slow self-discharge. *Nat. Commun.* **6**, 7818 (2015).

Acknowledgements
The authors thank E. Arzt (INM) for his continued support for research on energy materials and electrochemical technologies. V.P. acknowledges funding from the German Research Foundation (Deutsche Forschungsgemeinschaft) through the MXene-CDI project (PR-1173/11), the Leibniz Association through the Carbon Metal-Oxide Nanohybrids project (CarMON) (SAW-2017) and the Minerva Foundation through an Award for Research Cooperation and High Excellence in Science (ARCHES). X.S. acknowledges financial support from the University of Illinois at Urbana–Champaign and the Department of Chemical and Biomolecular Engineering, and the support of the National Science Foundation under CBET grant no. 1931941.

Author contributions
All authors contributed equally to the preparation of this manuscript.

Competing interests
The authors declare no competing interests.

Publisher's note
Springer Nature remains neutral with regard to jurisdictional claims in published maps and institutional affiliations.